

Anisotropic Topological Anderson Transitions in Chiral Symmetry Classes

Zhenyu Xiao,¹ Kohei Kawabata,^{2,3} Xunlong Luo,⁴ Tomi Ohtsuki,⁵ and Ryuichi Shindou^{1,*}

¹International Center for Quantum Materials, Peking University, Beijing 100871, China

²Department of Physics, Princeton University, Princeton, New Jersey 08544, USA

³Institute for Solid State Physics, University of Tokyo, Kashiwa, Chiba 277-8581, Japan

⁴Science and Technology on Surface Physics and Chemistry Laboratory, Mianyang 621907, China

⁵Physics Division, Sophia University, Chiyoda-ku, Tokyo 102-8554, Japan

(Dated: August 1, 2023)

We study quantum phase transitions of three-dimensional disordered systems in the chiral classes (AIII and BDI) with and without weak topological indices. We show that the systems with a non-trivial weak topological index universally exhibit an emergent thermodynamic phase where wave functions are delocalized along one spatial direction but exponentially localized in the other two spatial directions, which we call the quasi-localized phase. Our extensive numerical study clarifies that the critical exponent of the Anderson transition between the metallic and quasi-localized phases, as well as that between the quasi-localized and localized phases, are different from that with no weak topological index, signaling the new universality classes induced by topology. The quasi-localized phase and concomitant topological Anderson transition manifest themselves in the anisotropic transport phenomena of disordered weak topological insulators and nodal-line semimetals, which exhibit the metallic behavior in one direction but the insulating behavior in the other directions.

Introduction—The last decades have seen remarkable discoveries of topological materials [1–3]. The interplay of disorder and topology leads to new types of quantum phase transitions, including the quantum Hall plateau transitions [4–13]. The universality classes of the disorder-driven metal-insulator transitions, known as the Anderson transitions, are characterized by the critical exponents and scaling functions, which are commonly believed to be determined solely by symmetry and spatial dimensions [14]. Many theories investigated whether topology can change the universality classes of the Anderson transitions [15–34]. Still, the role of topology in the Anderson transitions has been elusive.

Prime examples of three-dimensional (3D) topological materials include nodal-line semimetals characterized by the weak topological invariant [35–38]. Several recent experiments realized nodal-line semimetals in solid states [39–41], as well as synthetic materials of ultracold atoms [42] and photonic [43, 44] and phononic [45] systems. Despite the significant interest in the physics of nodal-line semimetals [46–50], their unique transport signatures have remained largely unexplored.

In this Letter, we elucidate that the weak topological indices induce a novel thermodynamic phase in 3D disordered systems, including topological nodal-line semimetals, in the chiral classes. There, 3D wave functions are delocalized along one spatial direction and exponentially localized along the other two spatial directions—quasi-localized phase [Fig. 1(a)]. From extensive numerical calculations, we evaluate correlation-length critical exponents of the Anderson transitions among the metallic, quasi-localized, and localized phases [Fig. 1(a)] and find that they are distinct from the critical exponent in topo-

logically trivial systems [Fig. 1(b)], signaling new universality classes induced by the topological indices. Notably, our quasi-localized phase and concomitant topological Anderson transition are of direct experimental relevance in the anisotropic transport that exhibits the metallic behavior in one direction but the insulating behavior in the other directions. While such anisotropic transport has played an important role in condensed matter physics [51–58], our results provide its new universal mechanism induced by the interplay of disorder and topology.

Lyapunov exponents and topological indices—We study disorder-induced quantum phase transitions of 3D chiral-symmetric Hamiltonians \mathcal{H} . The localization properties along the μ direction ($\mu = x, y, z$) are efficiently captured by the Lyapunov exponents (LEs) along the μ direction

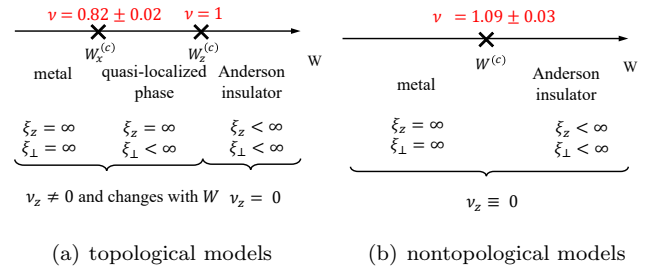


FIG. 1. Phase diagrams of 3D disordered Hamiltonians in the chiral symmetry classes (a) with and (b) without the weak topological index ν_z . The critical exponents ν and localization lengths ξ_z, ξ_\perp ($\perp = x, y$) along different directions are shown for different phases. The nontrivial critical exponents $\nu = 0.82 \pm 0.02$ and $\nu = 1.09 \pm 0.03$ are obtained for class BDI.

* rshindou@pku.edu.cn

in the limit $L \rightarrow \infty$, which are eigenvalues of [59, 60]

$$\lim_{L_\mu \rightarrow \infty} \log(M^\dagger M)^{\frac{1}{2L_\mu}}. \quad (1)$$

Here, $M \equiv M_{L_\mu} M_{L_\mu-1} \cdots M_1$ is the product of transfer matrices along the μ direction. The smallest positive LE gives the inverse of the localization length along the μ direction [61]. In the limit $L \rightarrow \infty$, the LEs of \mathcal{H} form several continuous spectra [62]. If the spectra do not include zero, the wave function is localized along the μ direction. By contrast, if the spectra include zero, the localization length diverges, which means the delocalization of the wave function. The finite (infinite) localization length leads to the vanishing (nonvanishing) conductance in the same direction, as shown in the Supplemental Material [34].

Symmetries of Hamiltonians give constraints on the spectrum of the LEs. For example, because of Hermiticity of \mathcal{H} , the LEs come in opposite-sign pairs. Moreover, in the presence of chiral symmetry, \mathcal{H} can be brought into the block off-diagonal structure,

$$\mathcal{H} = \begin{pmatrix} 0 & h \\ h^\dagger & 0 \end{pmatrix}, \quad (2)$$

where the off-diagonal part h is assumed to be a square matrix. Because of chiral symmetry, the LEs of \mathcal{H} reduce to the LEs of h and h^\dagger , which come in opposite-sign pairs, as shown in the Supplemental Material [34]. Consequently, we only need to calculate the product of the transfer matrices of h .

We demonstrate that a weak topological index ν_μ imposes another constraint on the spectrum of the LEs and plays a vital role in the emergence of the quasi-localized phase in disordered chiral-symmetric systems. To introduce ν_μ along the μ direction in the presence of disorder, let us insert a magnetic flux ϕ_μ through a closed loop along the μ direction. Then, the weak topological index ν_μ is given by the winding of $\det h(\phi_\mu)$ in Eq. (2) under an adiabatic insertion of a unit flux [63–65]:

$$\nu_\mu \equiv \frac{i}{L^2} \int_0^{2\pi} \frac{d\phi_\mu}{2\pi} \partial_{\phi_\mu} \text{Tr}[\log[h(\phi_\mu)]], \quad (3)$$

where L^2 is the system size within the two directions perpendicular to the μ direction. Here, ν_μ is not necessarily quantized and takes an arbitrary real number. Notably, the weak topological index ν_μ and LEs of h are related to each other by [34, 66]

$$\nu_\mu = \frac{1}{2L^2} (N_{+,\mu} - N_{-,\mu}), \quad (4)$$

where $N_{+,\mu}$ and $N_{-,\mu}$ are the numbers of positive and negative LEs of h along the μ direction, respectively.

Suppose \mathcal{H} has a mobility gap around $E = 0$ and its zero-energy state is characterized by the weak topological indices $\nu_x = \nu_y = 0$, $\nu_z = 1$. From Eq. (4), a finite gap exists between the smallest positive LE and the largest

negative LE such that $N_{+,z} - N_{-,z} = 2L^2$. By contrast, when disorder is strong enough, the zero-energy state is in a topologically-trivial localized phase with $N_{+,z} = N_{-,z}$. Between the two localized phases, L^2 positive LEs of h cross zero, and ν_z continuously changes from 1 to 0 with respect to the disorder strength, where the localization length ξ_z along the z direction always diverges. Within this finite range with divergent ξ_z , the zero-energy state undergoes the Anderson transitions along the x and y directions, and thus a quasi-localized phase with divergent ξ_z and finite ξ_x and ξ_y emerges. Below, we clarify its nature, obtain the critical exponents of the Anderson transitions among the metallic, quasi-localized, and localized phases, and demonstrate the existence of new universality classes.

Model—As a prototypical example, we study a two-orbital tight-binding model on a 3D cubic lattice [50]

$$\mathcal{H} = \sum_{\mathbf{r}=(r_x, r_y, r_z)} \left\{ \epsilon_{\mathbf{r}} c_{\mathbf{r}}^\dagger \sigma_z c_{\mathbf{r}} + \left[\sum_{\mu=x,y} (t_\perp c_{\mathbf{r}+\mathbf{e}_\mu}^\dagger \sigma_z c_{\mathbf{r}}) - it_\parallel c_{\mathbf{r}+\mathbf{e}_z}^\dagger \sigma_y c_{\mathbf{r}} + t'_\parallel c_{\mathbf{r}+\mathbf{e}_z}^\dagger \sigma_z c_{\mathbf{r}} + \text{H.c.} \right] \right\}. \quad (5)$$

Here, $c_{\mathbf{r}}$ is a two-component annihilation operator at the cubic lattice site \mathbf{r} , σ_μ ($\mu = x, y, z$) are Pauli matrices, t_\perp , t_\parallel , t'_\parallel are real-valued parameters, and $\epsilon_{\mathbf{r}}$ is a random potential that distributes uniformly in $[-W/2, W/2]$. We assume $t_\perp, t_\parallel > 0$ for simplicity. This Hamiltonian respects time-reversal symmetry $\mathcal{H} = \mathcal{H}^*$ and chiral symmetry $\mathcal{H} = -\sigma_x \mathcal{H} \sigma_x$, and hence belongs to class BDI [3, 14, 67]. In addition, the ensemble of Hamiltonians is statistically invariant under the combination of time reversal and reflection with respect to the xy plane, which requires $N_{+,x} = N_{-,x}$, $N_{+,y} = N_{-,y}$ and $\nu_x = \nu_y = 0$, as shown in the Supplemental Material [34], while ν_z can be nonzero. In the clean limit, the Hamiltonian has an energy gap around $E = 0$ with $\nu_z = 1$ for $4t_\perp < 2|t'_\parallel|$. For $4t_\perp > 2|t'_\parallel|$, by contrast, the zero-energy state forms a nodal line in momentum space, resulting in $0 < \nu_z < 1$. In the following, we focus on the nodal-line-semimetal phase for $t_\parallel = t'_\parallel = 1/2$, $t_\perp = 1$ and study the Anderson transitions of the zero modes along all the directions. Still, we stress that the weak topological invariant ν_μ , rather than a nodal line itself, is the main ingredient for the quasi-localized phase.

Localization length ξ_z —Figure 2 shows the distribution of LEs γ of h in Eq. (2) for the nodal-line-semimetal model \mathcal{H} in Eq. (5) along the z direction in the quasi-1D geometry $L \times L \times L_z$. The distribution consists of two separate spectra, each of which contains L^2 LEs. The upper spectrum is always $\gamma = +\infty$ [34] and irrelevant to the Anderson transitions. For $W \leq W_c^{(z)} \approx 29$, the lower spectrum includes zero $\gamma = 0$. Every positive LE in the lower spectrum for $W < W_c^{(z)}$ crosses zero when we increase W . At each crossing point, $N_{-,z}$ changes by one. For $L \rightarrow \infty$, the crossing points become dense and $\nu_z = 1 - N_{-,z}/L^2$ changes continuously with W . For $W >$

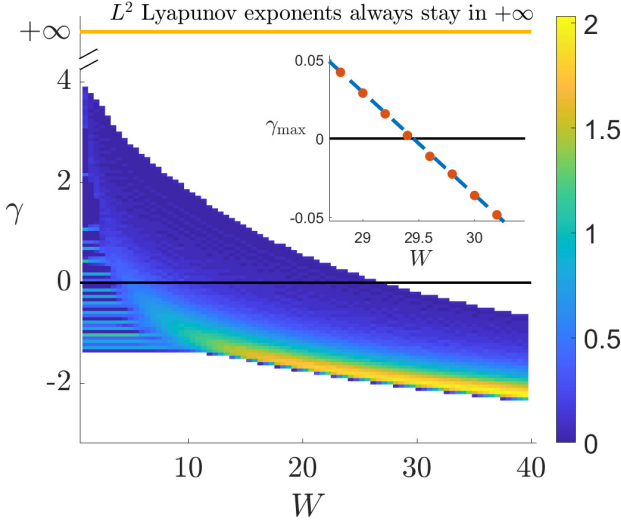


FIG. 2. $2L^2$ Lyapunov exponents (LEs) of the right-upper part h of the 3D nodal-line-semimetal model \mathcal{H} along the z direction with the quasi-1D geometry $L \times L \times L_z$ ($L = 18$, $L_z = 2 \times 10^6$), plotted as a function of the disorder strength W . The color scale stands for the density $\rho(\gamma)$ of the LEs with the normalization $\int \rho(\gamma) d\gamma = 1$. The LEs of \mathcal{H} are composed of the LEs of h and h^\dagger . Inset: the largest LE $\gamma_{\max}(W, L)$ among the smaller L^2 LEs as a function of W in the limit $L \rightarrow \infty$, obtained by a finite-size scaling fit. The error bars are smaller than the marks. The plot crosses zero linearly at $W_c^{(z)} = 29.45 \pm 0.05$; $\xi_z \sim (W - W_c^{(z)})^{-\nu'}$ with $\nu' = 1$ for $W > W_c^{(z)}$.

$W_c^{(z)}$, all the LEs in the lower spectrum are negative (i.e., $N_{-,z} = L^2$), and the system is in a localized phase with no weak topological index $\nu_z = 0$. At $W = W_c^{(z)}$, the maximal LE in the lower spectrum crosses zero. Notably, $W_c^{(z)}$ for $L \rightarrow \infty$ cannot be determined by fitting ξ_z/L with a standard scaling function [e.g., see Eq. (7)] because ξ_z with finite L diverges at some $W < W_c^{(z)}$. Instead, we map the non-Hermitian matrix h into a well-localized Hermitian matrix by a similarity transformation [34, 68], where the localization length obeys a scaling form in the strong disorder limit [69]. Then, we obtain the scaling form of the largest LE $\gamma_{\max}(W, L)$,

$$\gamma_{\max}(W, L) = a/L + \gamma_{\max}(W, L = \infty). \quad (6)$$

We numerically verify this scaling and determine the critical disorder strength $W_c^{(z)} = 29.45 \pm 0.05$ (inset of Fig. 2).

Localization length ξ_x, ξ_y —The statistical symmetries mentioned above require LEs of h along the x and y directions to come in opposite-sign pairs. Thus, the localization length ξ_x along the x direction is always finite in the quasi-1D geometry with finite L . As shown in Fig. 3, the normalized localization length $\Lambda_x(W, L) \equiv \xi_x(W, L)/L$ shows scale-invariant behavior at a certain disorder strength $W_c^{(x)}$ well below $W = W_c^{(z)}$, indicat-

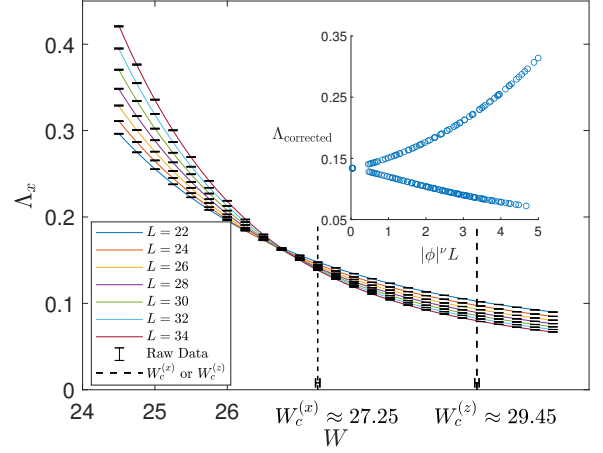


FIG. 3. Normalized localization length $\Lambda_x \equiv \xi_x/L$ along the x direction as a function of the disorder strength W in the nodal-line-semimetal model in Eq. (5) with the quasi-1D geometry $L \times L \times L_x$. The black points are the raw data with the error bars. The solid lines for different L and the dashed vertical line $W_c^{(x)}$ with the error bars are the results of the fitting according to Eq. (7) with $n = 3$. The dashed line $W_c^{(z)}$ is evaluated by the fitting of the Lyapunov exponent along the z direction by Eq. (6). Inset: single-parameter scaling function of Λ_x . $\Lambda_{\text{corrected}}$ is Λ_x subtracted by a contribution of the irrelevant scaling variable c in Eq. (7), and ϕ is the relevant scaling variable.

ing a quantum phase transition at $W = W_c^{(x)} < W_c^{(z)}$. To determine $W_c^{(x)}$ and the critical exponent ν , we use a finite-size scaling function and its polynomial expansion [61, 70]. The scaling function for $\Lambda_x(W, L)$ is Taylor-expanded with respect to the relevant scaling variable $\phi(w)$ and the least irrelevant scaling variable c up to the n th order and first order, respectively,

$$\Lambda_x(W, L) = \sum_{i=0}^n \sum_{j=0}^1 a_{i,j} (\phi(w) L^{1/\nu})^i (c L^{-y})^j, \quad (7)$$

with $w \equiv (W - W_c^{(x)})/W_c^{(x)}$ and the scaling dimension $-y$ (< 0) of the least irrelevant scaling variable around a saddle-point fixed point. The fitting is carried out by the χ^2 fitting method, and the confidence error bars for the optimal parameters are determined by the Monte Carlo method, as detailed in the Supplemental Material [34].

The first row in Table I shows the fitting results, where $W_c^{(x)} = 27.24 \pm 0.05$ is significantly smaller than $W_c^{(z)} = 29.45 \pm 0.05$ and the critical exponent at $W_c^{(x)}$ is evaluated as $\nu = 0.82 \pm 0.02$. The two different critical disorder strengths illustrate the emergence of the three distinct phases as a function of the disorder strength W [Fig. 1(a)]. For $W < W_c^{(x)}$, the localization lengths along all directions (metallic phase). For $W > W_c^{(z)}$, the localization lengths are finite along all directions (Anderson insulator phase). For

TABLE I. Critical disorder strength $W_c^{(\mu)}$ and critical exponent ν for the 3D chiral classes, obtained by the polynomial fitting of the normalized localization length $\Lambda_\mu \equiv \xi_\mu/L$ along the μ direction ($\mu = x, y, z$) around critical points of different models with the quasi-one-dimensional geometry $L \times L \times L_\mu$. In the column “Topo”, “ \checkmark ” shows the nonzero weak topological index ν_z around the critical point, and “ \times ” shows zero topological indices in all the directions. The square brackets denote the 95% confidence interval.

Class	Topo	μ	$W_c^{(\mu)}$	ν
BDI	\checkmark	x	27.241[27.194,27.303]	0.820[0.783,0.846]
AIII	\checkmark	x	9.143[9.125,9.168]	0.824[0.776,0.862]
BDI	\times	z	23.220[23.167,23.293]	1.089[1.005,1.128]
BDI	\times	x	23.170[23.098,23.279]	1.042[0.943,1.099]
AIII	\times	z	8.091[8.074,8.096]	1.024[0.973,1.070]

$W_c^{(x)} < W < W_c^{(z)}$, the localization lengths are finite along the x and y directions but diverge along the z direction (quasi-localized phase), and ν_z continuously changes as W changes. Our extensive numerical calculations show that the quasi-localized phase with divergent ξ_z but finite ξ_x, ξ_y universally appears between metallic and localized phases in different models with nonzero ν_z , as shown in the Supplemental Material [34]. The consistent critical exponent at $W = W_c^{(x)}$ was also obtained in Ref. [50], while a different critical exponent was obtained in Ref. [71] even in the same class. In this Letter, we elucidate that this difference originates from the emergence of the quasi-localized phase, which was not identified previously.

Quasi-localized phase—Now, we clarify the nature of the quasi-localized phase induced by the weak topological index ν_μ . Let $\Phi(\mathbf{r}) = \langle \mathbf{r} | \Phi \rangle$ be a normalized wave function. The wave function interacts with an effective disorder potential $V_{\text{eff}} = \langle \Phi | V | \Phi \rangle = \sum_{\mathbf{r}} V(\mathbf{r}) |\Phi(\mathbf{r})|^2$, whose strength is given by $\langle V_{\text{eff}}^2 \rangle = W^2 P_2$ with the inverse participation ratio $P_2 \equiv \sum_{\mathbf{r}} |\Phi(\mathbf{r})|^4$. Here, $\langle \dots \rangle$ denotes the disorder average: $\langle V(\mathbf{r}) V(\mathbf{r}') \rangle = W^2 \delta_{\mathbf{r}, \mathbf{r}'}$. As long as W is finite, the following argument is applicable to general $V(\mathbf{r})$, including the box disorder in $[-W/2, W/2]$ used for the numerical calculations. Let us introduce the integrated weight of the wave function in the z th layer by $|\phi(z)|^2 = \sum_{x,y} |\Phi(\mathbf{r})|^2$ and also the one-dimensional inverse participation ratio $P_2^z \equiv \sum_z |\phi(z)|^4$. P_2^x, P_2^y can be defined in the same manner. P_2^μ measures the localization property of $\Phi(\mathbf{r})$ along the μ direction, giving an upper bound of P_2 : $P_2 \leq P_2^\mu$ ($\mu = x, y, z$) [34]. If the wave function is extended along the z direction (i.e., $P_2^z \sim L_z^{-1}$ [14]), P_2 and $\langle V_{\text{eff}}^2 \rangle$ should vanish for $L_z \rightarrow \infty$, and $\Phi(\mathbf{r})$ must be extended along all the directions. If P_2^z is finite even for $L_z \rightarrow \infty$, by contrast, P_2^x and P_2^y should also be finite for $L_x, L_y \rightarrow \infty$. Otherwise, $\Phi(\mathbf{r})$ is extended within all the directions, which contradicts finite P_2^z . In the intermediate phase discussed above, we find that ξ_x is finite but ξ_z diverges. While finite ξ_x means finite P_2 and P_2^z , divergent ξ_z with finite P_2^z means that the wave function $\Phi(\mathbf{r})$ must be quasi-localized along the

z direction. Thus, the wave function in the intermediate phase is localized within the xy plane and delocalized only along the z direction—quasi-localized phase. Here, $\Phi(\mathbf{r})$ along the z direction shares the same localization properties as wave functions of 1D chiral-symmetric systems at a topological phase transition, where the 1D topological index changes [14, 63, 64, 72–74]. The 3D system in the intermediate phase is effectively decoupled into 1D wires because of finite $\xi_{x,y}$.

The emergence of the quasi-localized phase in 3D systems is a consequence of finite P_2^{1D} at the topological phase transition of 1D chiral-symmetric systems. Generally, when a d' -dimensional wave function $\Phi(\mathbf{R})$ in $\mathbf{R} \equiv (\mathbf{r}, \mathbf{s})$ with $\mathbf{r} = (r_1, \dots, r_d)$ and $\mathbf{s} = (s_1, \dots, s_{d'-d})$ ($d < d'$) is made out of coupled d -dimensional wave functions $\psi(\mathbf{r})$ at a critical point, $\Phi(\mathbf{R})$ is more extended than $\psi(\mathbf{r})$ along the \mathbf{r} direction because of the interlayer coupling [34]. Thus, the effective disorder strength for the d' -dimensional wave function $\Phi(\mathbf{R})$ is bounded by the d -dimensional inverse participation ratio $P_2^{\psi(\mathbf{r})}$ of $\psi(\mathbf{r})$. When the wave function $\psi(\mathbf{r})$ has finite $P_2^{\psi(\mathbf{r})}$ at the critical point, the effective disorder strength can be finite, and $\Phi(\mathbf{R})$ can be either extended or localized within the \mathbf{s} direction. On the other hand, when $P_2^{\psi(\mathbf{r})}$ is zero at the critical point, e.g., 2D critical wave functions at the quantum Hall plateau transition, the effective disorder strength is zero, and the d' -dimensional wave function should be always extended in both \mathbf{r} and \mathbf{s} directions. Notably, the 1D topological phase transitions in all the three chiral classes are characterized by finite P_2 [14]. In the following, we demonstrate the quasi-localized phases also in the 3D chiral unitary class, which is consistent with the above argument.

Model without time-reversal symmetry—We add a time-reversal-breaking but chiral-symmetric disorder $\Delta\mathcal{H}$ to the model \mathcal{H} in Eq. (5):

$$\mathcal{H}_1 = \mathcal{H} + \Delta\mathcal{H}, \quad \Delta\mathcal{H} = \sum_{\mathbf{r}} \epsilon'_{\mathbf{r}} c_{\mathbf{r}}^\dagger \sigma_y c_{\mathbf{r}}, \quad (8)$$

with the random potentials $\epsilon'_{\mathbf{r}}$, where $(\epsilon_{\mathbf{r}}, \epsilon'_{\mathbf{r}}) = (V_{\mathbf{r}} \cos \theta_{\mathbf{r}}, V_{\mathbf{r}} \sin \theta_{\mathbf{r}})$, and $\theta_{\mathbf{r}}$ and $V_{\mathbf{r}}$ distribute uniformly in the range of $[0, 2\pi)$ and $[0, W]$, respectively. This model only respects chiral symmetry and belongs to class AIII, in which the weak topological indices are defined in the same manner. It shows a similar phase diagram as in the previous model in class BDI with $W_c^{(z)} = 9.8 \pm 0.1$ and $W_c^{(x)} = 9.14 \pm 0.01$ (see Fig. 1 and Table I). The critical exponents are the same as those in the models in class BDI, which suggests possible super-universality in 3D systems in the chiral classes with the topological indices.

Models with trivial topological indices—To further clarify the role of the topological indices, we also study a topologically trivial model in class BDI with statistical symmetries. The statistical symmetry of time reversal combined with reflection with respect to the xz or yz plane makes all three topological indices vanish, as

shown in the Supplemental Material [34]. In addition, LEs of h along any direction come in opposite-sign pairs, and the localization lengths along the x and y directions are the same. On increasing the disorder strength, the model undergoes the Anderson transition, where the normalized localization lengths Λ_x and Λ_z along the x and z directions both show scale-invariant behaviors. The critical disorder strengths and critical exponents determined from Λ_x and Λ_z are consistent with each other (see Table I), which suggests that the scale-invariant behavior of Λ_x and Λ_z comes from the same quantum phase transition [Fig. 1(b)]. The evaluated critical exponent $\nu = 1.089[1.005, 1.128]$ is different from ν at $W = W_c^{(x)}$ of the topological model, and consistent with ν of the topologically trivial models in Ref. [71]. We also evaluate the critical exponent in the chiral unitary class without weak topological indices as $\nu = 1.024[0.973, 1.070]$ (Table I), which is different from ν of the topological models in the same symmetry class and consistent with Refs. [33, 71].

Summary and discussion—In this Letter, we show that in 3D systems in the chiral classes, the weak topological indices induce a disorder-driven quasi-localized phase where wave functions are delocalized only along one direction and localized along the other two directions. The critical exponents of the Anderson transitions among metal, quasi-localized, and localized phases are all different (Fig. 1). We believe that these conclusions hold also in the chiral symplectic class (class CII). Our quasi-localized phase leads to the anisotropic transport phenomena of topological nodal-line semimetals [36–45], where the conductance along the direction with the divergent localization length takes finite values with larger fluctuations, while it vanishes along the other directions

in the thermodynamic limit, as shown in the Supplemental Material [34]. The quasi-localized phase may potentially find practical applications such as quantum devices that control the direction of currents.

Our results are also relevant to non-Hermitian physics [75–77], where the interplay between disorder and dissipation has recently acquired renewed interest. In fact, all the disorder-driven phases and phase transitions in this Letter are characterized by the LEs of the off-diagonal part h in Eq. (2), which can be considered as a non-Hermitian Hamiltonian [33]. Anisotropy of \mathcal{H} corresponds to nonreciprocity of h and leads to transport phenomena unique to open systems.

3D chiral-symmetric systems also host a strong topological index [1–3]. By a similar numerical study, we find that the strong index does not lead to the quasi-localized phases, not influencing the universality classes of the Anderson transitions [78]. It also remains to be explored whether the quasi-localized phase appears and whether the topological indices change the universality classes of the Anderson transitions in 2D systems, as well as nodal-line semimetals protected by spatial symmetry.

Acknowledgement—Z.X. thanks Zhida Song, Lingxian Kong, and Yeyang Zhang for fruitful discussions. Z.X. and R.S. were supported by the National Basic Research Programs of China (No. 2019YFA0308401) and by National Natural Science Foundation of China (No. 11674011 and No. 12074008). K.K. was supported by JSPS Overseas Research Fellowship, and Grant No. GBMF8685 from the Gordon and Betty Moore Foundation toward the Princeton theory program. X.L. was supported by National Natural Science Foundation of China of Grant No. 12105253. T.O. was supported by JSPS KAKENHI Grant 19H00658 and 22H05114.

-
- [1] M. Z. Hasan and C. L. Kane, Colloquium: Topological insulators, *Rev. Mod. Phys.* **82**, 3045 (2010).
 - [2] X.-L. Qi and S.-C. Zhang, Topological insulators and superconductors, *Rev. Mod. Phys.* **83**, 1057 (2011).
 - [3] C.-K. Chiu, J. C. Y. Teo, A. P. Schnyder, and S. Ryu, Classification of topological quantum matter with symmetries, *Rev. Mod. Phys.* **88**, 035005 (2016).
 - [4] K. v. Klitzing, G. Dorda, and M. Pepper, New Method for High-Accuracy Determination of the Fine-Structure Constant Based on Quantized Hall Resistance, *Phys. Rev. Lett.* **45**, 494 (1980).
 - [5] J. Chalker and P. Coddington, Percolation, quantum tunnelling and the integer Hall effect, *J. Phys. C* **21**, 2665 (1988).
 - [6] A. M. M. Pruisken, Universal Singularities in the Integral Quantum Hall Effect, *Phys. Rev. Lett.* **61**, 1297 (1988).
 - [7] B. Huckestein, Scaling theory of the integer quantum Hall effect, *Rev. Mod. Phys.* **67**, 357 (1995).
 - [8] M. J. Bhaseen, I. I. Kogan, O. A. Soloviev, N. Taniguchi, and A. M. Tsvelik, Towards a field theory of the plateau transitions in the integer quantum Hall effect, *Nucl. Phys. B* **580**, 688 (2000).
 - [9] K. Slevin and T. Ohtsuki, Critical exponent for the quantum Hall transition, *Phys. Rev. B* **80**, 041304 (2009).
 - [10] E. Prodan, T. L. Hughes, and B. A. Bernevig, Entanglement Spectrum of a Disordered Topological Chern Insulator, *Phys. Rev. Lett.* **105**, 115501 (2010).
 - [11] Q. Zhu, P. Wu, R. N. Bhatt, and X. Wan, Localization-length exponent in two models of quantum Hall plateau transitions, *Phys. Rev. B* **99**, 024205 (2019).
 - [12] M. Puschmann, P. Cain, M. Schreiber, and T. Vojta, Integer quantum Hall transition on a tight-binding lattice, *Phys. Rev. B* **99**, 121301 (2019).
 - [13] E. J. Dresselhaus, B. Sbierski, and I. A. Gruzberg, Scaling Collapse of Longitudinal Conductance near the Integer Quantum Hall Transition, *Phys. Rev. Lett.* **129**, 026801 (2022).
 - [14] F. Evers and A. D. Mirlin, Anderson transitions, *Rev. Mod. Phys.* **80**, 1355 (2008).
 - [15] Y. Asada, K. Slevin, and T. Ohtsuki, Anderson Transition in Two-Dimensional Systems with Spin-Orbit Coupling, *Phys. Rev. Lett.* **89**, 256601 (2002).
 - [16] Y. Asada, K. Slevin, and T. Ohtsuki, Anderson Transition in the Three Dimensional Symplectic Universality

- Class, J. Phys. Soc. Jpn. **74**, 238 (2005).
- [17] M. Onoda, Y. Avishai, and N. Nagaosa, Localization in a Quantum Spin Hall System, Phys. Rev. Lett. **98**, 076802 (2007).
 - [18] H. Obuse, A. Furusaki, S. Ryu, and C. Mudry, Two-dimensional spin-filtered chiral network model for the \mathbb{Z}_2 quantum spin-Hall effect, Phys. Rev. B **76**, 075301 (2007).
 - [19] S. Ryu, C. Mudry, H. Obuse, and A. Furusaki, \mathbb{Z}_2 Topological Term, the Global Anomaly, and the Two-Dimensional Symplectic Symmetry Class of Anderson Localization, Phys. Rev. Lett. **99**, 116601 (2007).
 - [20] K. Nomura, M. Koshino, and S. Ryu, Topological Delocalization of Two-Dimensional Massless Dirac Fermions, Phys. Rev. Lett. **99**, 146806 (2007).
 - [21] A. D. Mirlin, F. Evers, I. V. Gornyi, and P. M. Ostrovsky, Anderson Transitions: Criticality, Symmetries, and Topologies, Int. J. Mod. Phys. B **24**, 1577 (2010).
 - [22] E. J. König, P. M. Ostrovsky, I. V. Protopopov, and A. D. Mirlin, Metal-insulator transition in two-dimensional random fermion systems of chiral symmetry classes, Phys. Rev. B **85**, 195130 (2012).
 - [23] Z. Ringel, Y. E. Kraus, and A. Stern, Strong side of weak topological insulators, Phys. Rev. B **86**, 045102 (2012).
 - [24] L. Fu and C. L. Kane, Topology, Delocalization via Average Symmetry and the Symplectic Anderson Transition, Phys. Rev. Lett. **109**, 246605 (2012).
 - [25] K. Slevin and T. Ohtsuki, Estimate of the Critical Exponent of the Anderson Transition in the Three and Four-Dimensional Unitary Universality Classes, J. Phys. Soc. Jpn. **85**, 104712 (2016).
 - [26] B. Roy, Y. Alavirad, and J. D. Sau, Global Phase Diagram of a Three-Dimensional Dirty Topological Superconductor, Phys. Rev. Lett. **118**, 227002 (2017).
 - [27] X. Luo, B. Xu, T. Ohtsuki, and R. Shindou, Quantum multicriticality in disordered Weyl semimetals, Phys. Rev. B **97**, 045129 (2018).
 - [28] N. Yoshioka, Y. Akagi, and H. Katsura, Learning disordered topological phases by statistical recovery of symmetry, Phys. Rev. B **97**, 205110 (2018).
 - [29] Z.-D. Song, B. Lian, R. Queiroz, R. Ilan, B. A. Bernevig, and A. Stern, Delocalization Transition of a Disordered Axion Insulator, Phys. Rev. Lett. **127**, 016602 (2021).
 - [30] J. H. Son and S. Raghu, Three-dimensional network model for strong topological insulator transitions, Phys. Rev. B **104**, 125142 (2021).
 - [31] Z. Pan, T. Wang, T. Ohtsuki, and R. Shindou, Renormalization group analysis of Dirac fermions with a random mass, Phys. Rev. B **104**, 174205 (2021).
 - [32] T. Wang, Z. Pan, T. Ohtsuki, I. A. Gruzberg, and R. Shindou, Multicriticality of two-dimensional class-D disordered topological superconductors, Phys. Rev. B **104**, 184201 (2021).
 - [33] X. Luo, Z. Xiao, K. Kawabata, T. Ohtsuki, and R. Shindou, Unifying the Anderson transitions in Hermitian and non-Hermitian systems, Phys. Rev. Research **4**, L022035 (2022).
 - [34] See Supplemental Material for summary of known critical exponents in topological insulators, inverse participation ratio, transfer matrix analyses, a relation between weak topological indices and Lyapunov exponents, statistical symmetry, details of finite-size scaling analyses, quasi-localized phase in other topological models, Anderson transition in non-topological models, and detailed numerical results of conductance in metal, quasi-localized and Anderson localized phases, which includes Refs. [79–85].
 - [35] A. A. Burkov, M. D. Hook, and L. Balents, Topological nodal semimetals, Phys. Rev. B **84**, 235126 (2011).
 - [36] A. P. Schnyder and P. M. R. Brydon, Topological surface states in nodal superconductors, J. Phys.: Condens. Matter **27**, 243201 (2015).
 - [37] C. Fang, H. Weng, X. Dai, and Z. Fang, Topological nodal line semimetals, Chinese Phys. B **25**, 117106 (2016).
 - [38] N. P. Armitage, E. J. Mele, and A. Vishwanath, Weyl and Dirac semimetals in three-dimensional solids, Rev. Mod. Phys. **90**, 015001 (2018).
 - [39] G. Bian, T.-R. Chang, R. Sankar, S.-Y. Xu, H. Zheng, T. Neupert, C.-K. Chiu, S.-M. Huang, G. Chang, I. Belopolski, D. S. Sanchez, M. Neupane, N. Alidoust, C. Liu, B. Wang, C.-C. Lee, H.-T. Jeng, C. Zhang, Z. Yuan, S. Jia, A. Bansil, F. Chou, H. Lin, and M. Z. Hasan, Topological nodal-line fermions in spin-orbit metal PbTaSe₂, Nat. Commun. **7**, 10556 (2016).
 - [40] L. M. Schoop, M. N. Ali, C. Straßer, A. Topp, A. Varykhalov, D. Marchenko, V. Duppel, S. S. P. Parkin, B. V. Lotsch, and C. R. Ast, Dirac cone protected by non-symmorphic symmetry and three-dimensional Dirac line node in ZrSiS, Nat. Commun. **7**, 11696 (2016).
 - [41] C. Chen, X.-T. Zeng, Z. Chen, Y. X. Zhao, X.-L. Sheng, and S. A. Yang, Second-Order Real Nodal-Line Semimetal in Three-Dimensional Graphdiyne, Phys. Rev. Lett. **128**, 026405 (2022).
 - [42] B. Song, C. He, S. Niu, L. Zhang, Z. Ren, X.-J. Liu, and G.-B. Jo, Observation of nodal-line semimetal with ultracold fermions in an optical lattice, Nat. Phys. **15**, 911 (2019).
 - [43] W. Gao, B. Yang, Biao Tremain, H. Liu, Q. Guo, L. Xia, A. P. Hibbins, and S. Zhang, Experimental observation of photonic nodal line degeneracies in metacrystals, Nat. Commun. **9**, 950 (2018).
 - [44] L. Xia, Q. Guo, B. Yang, J. Han, C.-X. Liu, W. Zhang, and S. Zhang, Observation of Hourglass Nodal Lines in Photonics, Phys. Rev. Lett. **122**, 103903 (2019).
 - [45] W. Deng, J. Lu, F. Li, X. Huang, M. Yan, J. Ma, and Z. Liu, Nodal rings and drumhead surface states in phononic crystals, Nat. Commun. **10**, 1769 (2019).
 - [46] R. Nandkishore, Weyl and Dirac loop superconductors, Phys. Rev. B **93**, 020506 (2016).
 - [47] S. Sur and R. Nandkishore, Instabilities of Weyl loop semimetals, New J. Phys. **18**, 115006 (2016).
 - [48] S. V. Syzranov and B. Skinner, Electron transport in nodal-line semimetals, Phys. Rev. B **96**, 161105 (2017).
 - [49] M. Gonçalves, P. Ribeiro, E. V. Castro, and M. A. N. Araújo, Disorder-Driven Multifractality Transition in Weyl Nodal Loops, Phys. Rev. Lett. **124**, 136405 (2020).
 - [50] X. Luo, B. Xu, T. Ohtsuki, and R. Shindou, Critical behavior of Anderson transitions in three-dimensional orthogonal classes with particle-hole symmetries, Phys. Rev. B **101**, 020202 (2020).
 - [51] M. J. Cohen, L. B. Coleman, A. F. Garito, and A. J. Heeger, Electrical conductivity of tetrathiofulvalinium tetracyanoquinodimethan (TTF)(TCNQ), Phys. Rev. B **10**, 1298 (1974).
 - [52] M. P. Lilly, K. B. Cooper, J. P. Eisenstein, L. N. Pfeiffer, and K. W. West, Evidence for an Anisotropic State of Two-Dimensional Electrons in High Landau Levels, Phys. Rev. Lett. **82**, 394 (1999).
 - [53] R. R. Du, D. C. Tsui, H. L. Stormer, L. N. Pfeiffer,

- K. W. Baldwin, and K. W. West, Strongly anisotropic transport in higher two-dimensional Landau levels, *Solid State Commun.* **109**, 389 (1999).
- [54] Y. Ando, K. Segawa, S. Komiya, and A. N. Lavrov, Electrical Resistivity Anisotropy from Self-Organized One Dimensionality in High-Temperature Superconductors, *Phys. Rev. Lett.* **88**, 137005 (2002).
- [55] R. A. Borzi, S. A. Grigera, J. Farrell, R. S. Perry, S. J. S. Lister, S. L. Lee, D. A. Tennant, Y. Maeno, and A. P. Mackenzie, Formation of a Nematic Fluid at High Fields in $\text{Sr}_3\text{Ru}_2\text{O}_7$, *Science* **315**, 214 (2007).
- [56] V. Hinkov, D. Haug, B. Fauqué, P. Bourges, Y. Sidis, A. Ivanov, C. Bernhard, C. T. Lin, and B. Keimer, Electronic Liquid Crystal State in the High-Temperature Superconductor $\text{YBa}_2\text{Cu}_3\text{O}_{6.45}$, *Science* **319**, 597 (2008).
- [57] J.-H. Chu, J. G. Analytis, K. D. Greve, P. L. McMahon, Z. Islam, Y. Yamamoto, and I. R. Fisher, In-Plane Resistivity Anisotropy in an Underdoped Iron Arsenide Superconductor, *Science* **329**, 824 (2010).
- [58] E. Fradkin, S. A. Kivelson, M. J. Lawler, J. P. Eisenstein, and A. P. Mackenzie, Nematic Fermi Fluids in Condensed Matter Physics, *Annu. Rev. Condens. Matter Phys.* **1**, 153 (2010).
- [59] A. MacKinnon and B. Kramer, One-Parameter Scaling of Localization Length and Conductance in Disordered Systems, *Phys. Rev. Lett.* **47**, 1546 (1981).
- [60] A. MacKinnon and B. Kramer, The scaling theory of electrons in disordered solids: Additional numerical results, *Z. Physik B* **53**, 1 (1983).
- [61] K. Slevin and T. Ohtsuki, Critical exponent for the Anderson transition in the three-dimensional orthogonal universality class, *New J. Phys.* **16**, 015012 (2014).
- [62] P. Markos, Phenomenological theory of the metal-insulator transition, *J. Phys.: Condens. Matter* **7**, 8361 (1995).
- [63] I. Mondragon-Shem, T. L. Hughes, J. Song, and E. Prodan, Topological Criticality in the Chiral-Symmetric AIII Class at Strong Disorder, *Phys. Rev. Lett.* **113**, 046802 (2014).
- [64] A. Altland, D. Bagrets, L. Fritz, A. Kamenev, and H. Schmiedt, Quantum Criticality of Quasi-One-Dimensional Topological Anderson Insulators, *Phys. Rev. Lett.* **112**, 206602 (2014).
- [65] J. Claes and T. L. Hughes, Disorder driven phase transitions in weak AIII topological insulators, *Phys. Rev. B* **101**, 224201 (2020).
- [66] L. Molinari, Spectral duality and distribution of exponents for transfer matrices of block-tridiagonal Hamiltonians, *J. Phys. A* **36**, 4081 (2003).
- [67] A. Altland and M. R. Zirnbauer, Nonstandard symmetry classes in mesoscopic normal-superconducting hybrid structures, *Phys. Rev. B* **55**, 1142 (1997).
- [68] N. Hatano and D. R. Nelson, Localization Transitions in Non-Hermitian Quantum Mechanics, *Phys. Rev. Lett.* **77**, 570 (1996).
- [69] Y. Asada, K. Slevin, and T. Ohtsuki, Numerical estimation of the β function in two-dimensional systems with spin-orbit coupling, *Phys. Rev. B* **70**, 035115 (2004).
- [70] K. Slevin and T. Ohtsuki, Corrections to Scaling at the Anderson Transition, *Phys. Rev. Lett.* **82**, 382 (1999).
- [71] T. Wang, T. Ohtsuki, and R. Shindou, Universality classes of the Anderson transition in the three-dimensional symmetry classes AIII, BDI, C, D, and CI, *Phys. Rev. B* **104**, 014206 (2021).
- [72] L. Balents and M. P. A. Fisher, Delocalization transition via supersymmetry in one dimension, *Phys. Rev. B* **56**, 12970 (1997).
- [73] H. Mathur, Feynman's propagator applied to network models of localization, *Phys. Rev. B* **56**, 15794 (1997).
- [74] P. W. Brouwer, C. Mudry, B. D. Simons, and A. Altland, Delocalization in Coupled One-Dimensional Chains, *Phys. Rev. Lett.* **81**, 862 (1998).
- [75] V. V. Konotop, J. Yang, and D. A. Zezyulin, Nonlinear waves in \mathcal{PT} -symmetric systems, *Rev. Mod. Phys.* **88**, 035002 (2016).
- [76] L. Feng, R. El-Ganainy, and L. Ge, Non-Hermitian photonics based on parity-time symmetry, *Nat. Photon.* **11**, 752 (2017).
- [77] R. El-Ganainy, K. G. Makris, M. Khajavikhan, Z. H. Musslimani, S. Rotter, and D. N. Christodoulides, Non-Hermitian physics and \mathcal{PT} symmetry, *Nat. Phys.* **14**, 11 (2018).
- [78] Z. Xiao, K. Kawabata, X. Luo, T. Ohtsuki, and R. Shindou, unpublished.
- [79] A. Crisanti, G. Paladin, and A. Vulpiani, *Products of Random Matrices* (Springer, Berlin, Heidelberg, 1993).
- [80] K. Kawabata, K. Shiozaki, M. Ueda, and M. Sato, Symmetry and Topology in Non-Hermitian Physics, *Phys. Rev. X* **9**, 041015 (2019).
- [81] I. Goldhirsch, P.-L. Sulem, and S. A. Orszag, Stability and Lyapunov stability of dynamical systems: A differential approach and a numerical method, *Physica D* **27**, 311 (1987).
- [82] I. C. Fulga, A. R. Akhmerov, J. Tworzydło, B. Béri, and C. W. J. Beenakker, Thermal metal-insulator transition in a helical topological superconductor, *Phys. Rev. B* **86**, 054505 (2012).
- [83] L. Fu, C. L. Kane, and E. J. Mele, Topological Insulators in Three Dimensions, *Phys. Rev. Lett.* **98**, 106803 (2007).
- [84] J. B. Pendry, A. MacKinnon, and A. B. Pretre, Maximal fluctuations—A new phenomenon in disordered systems, *Physica A* **168**, 400 (1990).
- [85] B. Kramer, T. Ohtsuki, and S. Kettemann, Random network models and quantum phase transitions in two dimensions, *Phys. Rep.* **417**, 211 (2005).

I. SUPPLEMENTAL MATERIAL FOR “TOPOLOGICAL ANDERSON TRANSITIONS IN CHIRAL SYMMETRY CLASSES”

This Supplemental Material is organized as follows. In Sec. IA, we summarize known critical exponents between metal and topological-insulator phases and between metal and ordinary-insulator phases. In Sec. IB, we introduce the inverse participation ratio along different directions and prove that coupling among low-dimensional systems makes wave functions more extended even in the small coupling limit. In Sec. IC, we review the polynomial fitting of the finite-size scaling function and details of Table I in the main text. In Sec. ID, we introduce the transfer matrix method and explain properties of transfer matrices for chiral-symmetric Hamiltonians. In Sec. IE, we summarize a relation between weak topological indices and distributions of Lyapunov exponents (LEs). In Sec. IF, we show how statistical symmetries require the weak topological indices to be zero and LEs of the non-Hermitian matrix (right upper part of a chiral-symmetric Hamiltonian) to come in opposite-sign pairs. In Sec. IG, we summarize a scaling form for the maximal and minimal LEs within a continuum spectrum and show numerical fittings based on this scaling form. In Secs. IH and II, we provide detailed numerical studies of the criticality in chiral-symmetric models with and without non-trivial topological indices, respectively. In Sec. IJ, we provide detailed numerical results of the two-terminal conductance of the model with non-trivial topological indices. The conductance shows the anisotropic transport behavior in the quasi-localized phase.

CONTENTS

References	5
I. Supplemental Material for “Topological Anderson Transitions in Chiral Symmetry Classes”	8
A. Summary of known critical exponents	9
B. Inverse participation ratio	9
1. Inverse participation ratio along different directions	9
2. Wave-function hybridization and inverse participation ratio	10
C. Polynomial fitting	11
D. Transfer matrix, Lyapunov exponents, and localization length	11
1. Transfer matrix of a chiral-symmetric Hamiltonian	12
2. Transfer matrix of the nodal-line semimetal model	13
E. Weak topological indices and Lyapunov exponents	14
1. Winding number in the clean limit	16
F. Statistical symmetry	17
1. Statistical symmetry, Lyapunov exponents, and one-dimensional winding number	17
2. Statistical symmetry in the nodal-line semimetal model	18
G. Finite-size scaling of Lyapunov exponents	18
1. Numerical fitting	20
H. Quasi-localized phases in chiral-symmetric models with weak topological indices	22
1. Nodal-line semimetal in class AIII	22
2. Nodal-line semimetals in class BDI	24
3. Weak topological insulators and ordinary insulators in class BDI	27
I. Anderson transitions in chiral-symmetric models with no weak topological indices	29
1. Three-dimensional non-topological models in classes BDI and AIII	30
2. Another three-dimensional non-topological model in class AIII	31
J. Conductance and weak topological indices	32

A. Summary of known critical exponents

Table II summarizes known results of critical exponents of the Anderson transitions between metal and topological-insulator phases and between metal and trivial-insulator phases in the same spatial dimensions and symmetry classes. For each symmetry class and spatial dimensions, the evaluated critical exponents for the two types of the Anderson transitions are consistent with each other. However, the critical exponents between topological-insulator and trivial-insulator phases, as well as those between topological-semimetal and diffusive-metal phases, can be different from the ones in Table II. In our work, we focus on the Anderson transitions in the 3D chiral classes and demonstrate the different critical exponents due to the weak topological indices.

TABLE II. Correlation-length critical exponents of the Anderson transitions between metal and topological-insulator phases and those between metal and trivial-insulator phases in the same symmetry classes and spatial dimensions.

	Class	Metal-topological-insulator	Metal-trivial-insulator
2D	AII	2.74 ± 0.12 [18]	2.73 ± 0.02^a [15]
	D	$1.371[1.311, 1.437]^a$ [32]	$1.348[1.279, 1.402]^a$ [32]
	DIII	1.5 ± 0.1 [28]	1.5 ± 0.1 [28]
3D	A	$1.34[1.23, 1.53]^a$ [27] ^b	$1.443[1.437, 1.449]^a$ [25]
		1.42 ± 0.12 [29] ^c	
	AII	1.311 ± 0.033^a [30] ^d	1.375 ± 0.016^a [16]
	DIII	0.85 ± 0.05 [26]	$0.903[0.896, 0.908]^a$ [33]

^a 95% confidence interval.

^b Layered Chern insulator.

^c Axion insulator.

^d Reference [30] obtained the critical exponent between the metal and topological-insulator phases in a three-dimensional network model belonging to symmetry class AII. The critical exponent is different from the one between the metal and trivial-insulator phases in the same symmetry class and spatial dimensions obtained by the SU(2) model [16]. However, a more careful error analysis is needed, because system sizes in Ref. [30] may not be large enough (≤ 10), and the difference between the two exponents is small.

B. Inverse participation ratio

1. Inverse participation ratio along different directions

The inverse participation ratio P_2 measures localization properties of a wave function $\Phi(\mathbf{r})$ in d dimension, defined by

$$P_2 \equiv \sum_{\mathbf{r}} |\Phi(\mathbf{r})|^4 \quad (9)$$

with the normalization condition $\sum_{\mathbf{r}} |\Phi(\mathbf{r})|^2 = 1$. We have $P_2 \leq 1$, where the equality holds only when $\Phi(\mathbf{r})$ is fully localized at one lattice site. P_2 in extended and localized phases show the different scaling relations with the system size L ,

$$P_2 \sim \begin{cases} L^{-d} & [\Phi(\mathbf{r}) \text{ is extended}] , \\ \text{constant} < 1 & [\Phi(\mathbf{r}) \text{ is localized}] \end{cases} \quad (10)$$

for $L \rightarrow \infty$. The one-dimensional inverse participation ratio P_2^μ ($\mu = x, y, z$) measures localization properties of $\Phi(x, y, z)$ along the μ direction. The integrated weight of the wave function at z , $|\phi(z)|^2 \equiv \sum_{x,y} |\Phi(x, y, z)|^2$, is regarded as the squared one-dimensional normalized wave function along the z direction and describes how the three-dimensional wave function $\Phi(x, y, z)$ is localized along the z direction. Thus, the inverse participation ratio P_2^z along the z direction is introduced as

$$P_2^z = \sum_z |\phi(z)|^4 \quad , \quad |\phi(z)|^2 = \sum_{x,y} |\Phi(x, y, z)|^2 . \quad (11)$$

Notably, P_2^z provides an upper bound of P_2 ,

$$P_2 = \sum_z |\phi(z)|^4 \left[\sum_{x,y} \left| \frac{\Phi(\mathbf{r})}{\phi(z)} \right|^4 \right] \leq P_2^z , \quad (12)$$

where the equality holds only when we have $\sum_{x,y} |\Phi(\mathbf{r})/\phi(z)|^4 = 1$ for all z . The one-dimensional inverse participation ratio P_2^μ along the other two directions ($\mu = x, y$) is defined in the same manner. In a similar manner, the d -dimensional inverse participation ratio is defined for a normalized wave function in d' dimension ($d < d'$). For example, the following two-dimensional inverse participation ratio $P_2^{(x,y)}$ measures the localization properties of $\Phi(x, y, z)$ within the xy plane,

$$P_2^{(x,y)} \equiv \sum_{x,y} |\phi(x, y)|^4, \quad |\phi(x, y)|^2 = \sum_z |\Phi(x, y, z)|^2, \quad (13)$$

which satisfies

$$P_2 \leq P_2^{(x,y)}. \quad (14)$$

2. Wave-function hybridization and inverse participation ratio

Suppose that a d' -dimensional disordered non-interacting Hamiltonian $\mathcal{H}^{\mathbf{R}}$ in $\mathbf{R} \equiv (\mathbf{r}, \mathbf{s})$ with $\mathbf{r} = (r_1, \dots, r_d)$ and $\mathbf{s} = (s_1, \dots, s_{d'-d})$ ($d < d'$) consists of d -dimensional Hamiltonians $\mathcal{H}_s^{\mathbf{r}}$ at different \mathbf{s} and coupling \mathcal{H}' among the d -dimensional systems. On-site disorder potential $V(\mathbf{R})$ is chosen to distribute uniformly in the range $[-W/2, W/2]$ for all the lattice sites \mathbf{R} . Then, \mathbf{s} can be regarded as different disorder realizations from the same ensemble for the d -dimensional system with the disorder strength W . In this section, we show that even in the small coupling limit, an eigenstate $\Phi(\mathbf{R})$ of $\mathcal{H}^{\mathbf{R}}$ with eigenenergy E is more extended along the \mathbf{r} direction than an eigenstate $\psi(\mathbf{r})$ of $\mathcal{H}_s^{\mathbf{r}}$ with the same eigenenergy. Here, the small coupling limit means that the maximal eigenvalue of \mathcal{H}' is much smaller than the mean level spacing of $\mathcal{H}_s^{\mathbf{r}}$ around E .

For $\mathcal{H}' = 0$, eigenstates of $\mathcal{H}^{\mathbf{R}}$ are given by eigenstates of $\mathcal{H}_s^{\mathbf{r}}$. In the small coupling limit, we can treat \mathcal{H}' perturbatively. We introduce an energy window $[E - \Delta E, E + \Delta E]$ and choose ΔE to be small enough that each $\mathcal{H}_s^{\mathbf{r}}$ has at most one eigenstate $\psi_s(\mathbf{r})$ with eigenenergy E_s in the energy window and that we have $|E_s - E| \ll \Delta E$. In the small coupling limit, the maximal eigenvalue of \mathcal{H}' can be much smaller than ΔE . Thus, in the lowest order of degenerate perturbation theory, \mathcal{H}' does not mix unperturbed eigenstates inside the energy window with those outside the energy window, and an eigenstate $\Phi(\mathbf{R})$ of $\mathcal{H}^{\mathbf{R}}$ is given by a linear superposition of $\psi_s(\mathbf{r})$ over different \mathbf{s} ,

$$\Phi(\mathbf{r}, \mathbf{s}) = \sum_{\mathbf{s}'} a_{\mathbf{s}'} \psi_{\mathbf{s}'}(\mathbf{r}) \delta_{\mathbf{s}, \mathbf{s}'} = a_{\mathbf{s}} \psi_{\mathbf{s}}(\mathbf{r}), \quad (15)$$

where $\delta_{\mathbf{s}, \mathbf{s}'}$ is the Kronecker delta. Here, we impose the normalization conditions $\sum_{\mathbf{s}} |a_{\mathbf{s}}|^2 = 1$ and $\sum_{\mathbf{r}} |\psi_{\mathbf{s}}(\mathbf{r})|^2 = 1$, where we sum only over such \mathbf{s} that $\mathcal{H}_s^{\mathbf{r}}$ has an eigenenergy inside the window $[E - \Delta E, E + \Delta E]$. $a_{\mathbf{s}}$ is the \mathbf{s} -component of an eigenstate of an effective Hamiltonian $H^{\mathbf{R}}$ given as

$$(H^{\mathbf{R}})_{\mathbf{s}, \mathbf{s}'} = \sum_{\mathbf{r}} \sum_{\mathbf{r}'} \psi_{\mathbf{s}}^*(\mathbf{r}) (\mathcal{H}')_{\mathbf{r}, \mathbf{r}'} \psi_{\mathbf{s}'}(\mathbf{r}') + E_{\mathbf{s}} \delta_{\mathbf{s}, \mathbf{s}'}. \quad (16)$$

In the following, we show that the inverse participation ratio $P_2^{\mathbf{r}}$ of $\Phi(\mathbf{R})$ along the \mathbf{r} direction is always smaller than the d -dimensional inverse participation ratio of $\psi_s(\mathbf{r})$. The weight $|\phi(\mathbf{r}_0)|^2$ of the wave function $\Phi(\mathbf{R})$ on a hyperplane $\mathbf{r} = \mathbf{r}_0$ is given as

$$|\phi(\mathbf{r})|^2 = \sum_{\mathbf{s}} |\Phi(\mathbf{r}, \mathbf{s})|^2. \quad (17)$$

The inverse participation ratio $P_2^{\mathbf{r}}$ of $\Phi(\mathbf{R})$ along the \mathbf{r} direction measures the localization properties of $\Phi(\mathbf{R})$ within the \mathbf{r} direction and is given by the sum of the square of the weight over \mathbf{r} ,

$$\begin{aligned} P_2^{\mathbf{r}} &= \sum_{\mathbf{r}} |\phi(\mathbf{r})|^4 = \sum_{\mathbf{r}} \sum_{\mathbf{s}_1} \sum_{\mathbf{s}_2} |\Phi(\mathbf{r}, \mathbf{s}_1)|^2 |\Phi(\mathbf{r}, \mathbf{s}_2)|^2 = \sum_{\mathbf{s}_1} \sum_{\mathbf{s}_2} |a_{\mathbf{s}_1}|^2 |a_{\mathbf{s}_2}|^2 \left[\sum_{\mathbf{r}} |\psi_{\mathbf{s}_1}(\mathbf{r})|^2 |\psi_{\mathbf{s}_2}(\mathbf{r})|^2 \right] \\ &\leq \frac{1}{2} \sum_{\mathbf{s}_1} \sum_{\mathbf{s}_2} |a_{\mathbf{s}_1}|^2 |a_{\mathbf{s}_2}|^2 \sum_{\mathbf{r}} [|\psi_{\mathbf{s}_1}(\mathbf{r})|^4 + |\psi_{\mathbf{s}_2}(\mathbf{r})|^4] = \sum_{\mathbf{s}} |a_{\mathbf{s}}|^2 \sum_{\mathbf{r}} |\psi_{\mathbf{s}}(\mathbf{r})|^4. \end{aligned} \quad (18)$$

Here, the equality holds true only when we have $\psi_{\mathbf{s}_1}(\mathbf{r}) = \psi_{\mathbf{s}_2}(\mathbf{r})$ for all \mathbf{r} , \mathbf{s}_1 , and \mathbf{s}_2 . Notably, $\sum_{\mathbf{r}} |\psi_{\mathbf{s}}(\mathbf{r})|^4$ is the d -dimensional inverse participation ratio $P_2^{\psi_s(\mathbf{r})}$ of $\psi_s(\mathbf{r})$, and $\mathcal{H}_s^{\mathbf{r}}$ at different \mathbf{s} belongs to the same ensemble with

the same disorder strength W . In the thermodynamic limit ($N_{\mathbf{r}} \equiv \sum_{\mathbf{r}} \rightarrow \infty$), ΔE goes to zero as the mean level spacing goes to zero, and $P_2^{\psi_s(\mathbf{r})}$ at different \mathbf{s} takes the same value $P_2^{\psi(\mathbf{r})}$. Then, we have

$$P_2^{\mathbf{r}} \leq P_2^{\psi(\mathbf{r})} \sum_{\mathbf{s}} |a_{\mathbf{s}}|^2 = P_2^{\psi(\mathbf{r})}, \quad (19)$$

which proves that within the lowest order in \mathcal{H}' , the small coupling \mathcal{H}' among the d -dimensional systems always makes d -dimensional wave functions spatially more extended.

C. Polynomial fitting

In this section, we present more details about the polynomial fitting [Eq. (7) in the main text] of the normalized localization length $\Lambda_x(W, L) = \xi_x(W, L)/L$ and show details of Table I in the main text (see Table III). The scaling function for $\Lambda_x(W, L)$ is Taylor-expanded with respect to the relevant scaling variable $\phi(w)$ and the least irrelevant scaling variable $\psi(w)$ up to the n th order and first order, respectively,

$$\Lambda_x(W, L) = \sum_{i=0}^n \sum_{j=0}^1 a_{i,j} (\phi(w)L^{1/\nu})^i (\psi(w)L^{-y})^j, \quad (20)$$

with $w \equiv (W - W_c^{(x)})/W_c^{(x)}$, and the scaling dimension $-y$ (< 0) of the least irrelevant scaling variable around a saddle-point fixed point. The relevant scaling variable is further expanded around $w = 0$ up to the m th order, while only the zeroth-order in w is kept for the irrelevant scaling variable $\psi(w)$,

$$\phi(w) = \sum_{k=1}^m b_k w^k, \quad \psi(w) = c. \quad (21)$$

Here, $\{W_c^{(x)}, \nu, y, a_{i,j}, b_k, c\}$ are the fitting parameters. To avoid the ambiguity in the Taylor expansion of the scaling function, we should set $a_{0,1} = a_{1,0} = 1$. Thus, the number N_f of the free parameters in the fitting is $N_f = 2(n+1) + m + 2$. We minimize χ^2 statistics

$$\chi^2 = \sum_{j=1}^{N_D} \left(\frac{F_j - \Lambda_j}{\sigma_j} \right)^2, \quad (22)$$

where Λ_j and σ_j are the normalized localization length and its standard deviation for (W, L) evaluated by the transfer matrix method, respectively, F_j is the value of the polynomial fitting function for (W, L) , and N_D is the number of data points. The confidence error bars for the optimal parameters are determined by the fittings for 1000 sets of synthetic data for $\Lambda_x(W, L)$. The synthetic data are generated according to a standard deviation from the transfer matrix calculation.

D. Transfer matrix, Lyapunov exponents, and localization length

The transfer matrix method solves an eigenvalue problem of a non-interacting disordered Hamiltonian \mathcal{H} recursively. This method is efficient for obtaining the localization length along one spatial direction, which we call the μ direction in the following. In this formulation, the Hamiltonian is decomposed into a layer structure along the μ direction,

$$\mathcal{H}_{i,j} = H_i \delta_{i,j} + V_{i,i+1} \delta_{i,j-1} + V_{i,i-1} \delta_{i,j+1}, \quad (23)$$

where $i, j = 1, 2, \dots, L_\mu$ are indices of the layers, H_i is a block of matrix elements within the i th layer, and $V_{i,i\pm 1}$ is a block of matrix elements between the i th layer and the $(i\pm 1)$ th layer. The decomposition assumes that matrix elements appear only between the nearest neighboring layers or within each layer. In the presence of next-nearest hopping, one can redefine two neighboring layers as one layer. Let $H_i, V_{i,i\pm 1}$ be m by m matrices and $(\dots, A_{i-1}, A_i, A_{i+1}, \dots)^T$ be an eigenvector of \mathcal{H} for an eigenenergy E :

$$H_i A_i + V_{i,i-1} A_{i-1} + V_{i,i+1} A_{i+1} = E A_i. \quad (24)$$

TABLE III. Polynomial fitting results of the normalized localization length $\Lambda_\mu \equiv \xi_\mu/L$ along the μ direction ($\mu = x, y, z$) around critical points of different models with the quasi-one-dimensional geometry $L \times L \times L_\mu$. “ \checkmark ” in the column “topology” shows that the weak topological index ν_z is non-zero around the critical point, and “ \times ” shows that all the weak topological indices always vanish around the critical point. We show the critical disorder strength $W_c^{(\mu)}$, critical exponent ν , scaling dimension $-y$ of the least irrelevant scaling variable, critical localization length Λ_c , the goodness of fitting (GOF), and Taylor-expansion order of (m, n) in Eqs. (20) and (21). The square brackets denote the 95% confidence interval. Note that Λ_c ’s here are critical values in the presence of anisotropic spatial geometry and take non-universal values.

symmetry class	topology	direction	m	n	GOF	$W_c^{(\mu)}$	ν	y	Λ_c
BDI	\checkmark	$\mu = x$	2	3	0.15	27.241[27.194,27.303]	0.820[0.783,0.846]	2.584[2.175,2.955]	0.134[0.130,0.137]
BDI	\checkmark	$\mu = x$	3	3	0.14	27.243[27.192,27.301]	0.820[0.787,0.848]	2.574[2.212,2.947]	0.134[0.130,0.138]
AIII	\checkmark	$\mu = x$	3	3	0.47	9.143[9.125,9.168]	0.824[0.776,0.862]	2.157[1.727,2.519]	0.225[0.213,0.232]
BDI	\times	$\mu = z$	2	3	0.19	23.220[23.167,23.293]	1.089[1.005,1.128]	1.926[1.074,3.034]	0.374[0.352,0.385]
BDI	\times	$\mu = z$	3	3	0.18	23.223[23.138,23.409]	1.088[0.991,1.141]	1.906[0.604,3.677]	0.373[0.302,0.389]
BDI	\times	$\mu = x$	2	3	0.23	23.170[23.098,23.279]	1.042[0.943,1.099]	1.591[0.889,2.543]	0.281[0.254,0.293]
BDI	\times	$\mu = x$	3	3	0.31	23.167[23.101,23.310]	1.039[0.937,1.100]	1.607[0.753,2.425]	0.281[0.239,0.292]
AIII	\times	$\mu = z$	2	3	0.20	8.091[8.074,8.096]	1.024[0.973,1.070]	0.470[0.450,1.481]	0.650[0.639,0.706]

For simplicity, suppose that the disorder terms are present only in the diagonal matrix elements and that $V_{i,i-1} = V_+$ and $V_{i,i+1} = V_-$ are free from disorder. The eigenvectors are solved layer by layer recursively by a transfer matrix M_i ,

$$\begin{pmatrix} A_{i+1} \\ A_i \end{pmatrix} = M_i \begin{pmatrix} A_i \\ A_{i-1} \end{pmatrix}, \quad M_i \equiv \begin{pmatrix} -V_-^{-1}(H_i - E) & -V_-^{-1}V_+ \\ 1_{m \times m} & 0_{m \times m} \end{pmatrix}. \quad (25)$$

The product of the transfer matrices, $M = M_{L_\mu} M_{L_\mu-1} \cdots M_1$, relates the components of the eigenvector at the $(L_\mu + 1)$ th and L_μ th layers with the components at the first and zeroth layer. According to Oseledec’s theorem [79], the matrix

$$P(E) = \lim_{L_\mu \rightarrow \infty} \ln(M^\dagger M)^{\frac{1}{2L_\mu}} = - \lim_{L_\mu \rightarrow \infty} \ln(M^{-1} M^{-1\dagger})^{\frac{1}{2L_\mu}} \quad (26)$$

well converges in the limit $L_\mu \rightarrow \infty$. Eigenvalues of $P(E)$ are known as Lyapunov exponents (LEs). If \mathcal{H} is Hermitian, LEs come in opposite-sign pairs [79]. The inverse of the smallest positive or the largest negative LE corresponds to the localization length ξ_μ along the μ direction.

1. Transfer matrix of a chiral-symmetric Hamiltonian

Suppose that a $2n \times 2n$ Hermitian Hamiltonian \mathcal{H} satisfies chiral symmetry $\mathcal{C}\mathcal{H}\mathcal{C}^{-1} = -\mathcal{H}$ with a chiral operator \mathcal{C} satisfying $\mathcal{C}^2 = 1$. Eigenvalues of \mathcal{C} are ± 1 , the numbers of which are assumed to be the same. Then, the unitary matrix \mathcal{C} is diagonalized as $\mathcal{C} = \sum_{i=1}^n |v_i\rangle \langle v_i| - \sum_{i=1}^n |u_i\rangle \langle u_i|$. Here, $|v_1\rangle, \dots, |v_n\rangle$ and $|u_1\rangle, \dots, |u_n\rangle$ are eigenvectors of \mathcal{C} with eigenvalues $+1$ and -1 , respectively. Because of chiral symmetry, we have $\langle v_i | \mathcal{H} | v_j \rangle = \langle u_i | \mathcal{H} | u_j \rangle = 0$. Thus, the $2n \times 2n$ matrix \mathcal{H} is decomposed into two $n \times n$ matrices h and h' in the off-diagonal parts,

$$\mathcal{H} = \begin{pmatrix} 0 & h \\ h' & 0 \end{pmatrix}, \quad (27)$$

with

$$(h)_{i,j} = \langle v_i | \mathcal{H} | u_j \rangle, \quad (h')_{i,j} = \langle u_i | \mathcal{H} | v_j \rangle, \quad (28)$$

satisfying $h' = h^\dagger$.

Equation (28) does not determine h uniquely up to $n \times n$ unitary transformations, $h \rightarrow \mathcal{V}^\dagger h \mathcal{U}$, where the unitary transformations \mathcal{V} and \mathcal{U} change bases among the n -fold degenerate eigenstates of \mathcal{C} . Nonetheless, with a certain choice of the bases for $|v_1\rangle, \dots, |v_n\rangle$ and $|u_1\rangle, \dots, |u_n\rangle$, any Hermitian Hamiltonian with chiral symmetry can be decomposed into the off-diagonal form as Eq. (27). The off-diagonal parts thus introduced are non-Hermitian matrices, in general.

If the chiral operator \mathcal{C} is diagonal with respect to the layer index and its matrix elements do not depend on the layer index, the Hamiltonian H_i within the i th layer and the hopping matrix V_\pm between the i th layer and the $(i \pm 1)$ th layers also take the block off-diagonal structure,

$$H_i = \begin{pmatrix} 0 & \tilde{h}_i \\ \tilde{h}_i^\dagger & 0 \end{pmatrix}, \quad V_+ = \begin{pmatrix} 0 & v_+ \\ v_-^\dagger & 0 \end{pmatrix}, \quad V_- = \begin{pmatrix} 0 & v_- \\ v_+^\dagger & 0 \end{pmatrix}, \quad (29)$$

where v_{\pm} are free from the disorder and independent of the layer index. The transfer matrix $M_i^{(\mathcal{H})}$ of \mathcal{H} for zero energy $E = 0$ reads

$$M_i^{(\mathcal{H})} = \begin{pmatrix} -\begin{pmatrix} 0 & v_- \\ v_+^\dagger & 0 \end{pmatrix}^{-1} \begin{pmatrix} 0 & \tilde{h}_i \\ \tilde{h}_i^\dagger & 0 \end{pmatrix} - \begin{pmatrix} 0 & v_- \\ v_+^\dagger & 0 \end{pmatrix}^{-1} \begin{pmatrix} 0 & v_+ \\ v_-^\dagger & 0 \end{pmatrix} \\ 1 & 0 & 0 & 0 \\ 0 & 1 & 0 & 0 \end{pmatrix} \quad (30)$$

$$= \begin{pmatrix} -v_+^{\dagger-1} \tilde{h}_i^\dagger & 0 & -v_+^{\dagger-1} v_-^\dagger & 0 \\ 0 & -v_-^{-1} \tilde{h}_i & 0 & -v_-^{-1} v_+ \\ 1 & 0 & 0 & 0 \\ 0 & 1 & 0 & 0 \end{pmatrix}.$$

With a proper unitary transformation \mathcal{U} , the transfer matrix $M_i^{(\mathcal{H})}$ is block-diagonalized into M_i and M'_i ,

$$\mathcal{U}^\dagger M_i^{(\mathcal{H})} \mathcal{U} = \begin{pmatrix} M'_i & 0 \\ 0 & M_i \end{pmatrix}, \quad M'_i \equiv \begin{pmatrix} -v_+^{\dagger-1} \tilde{h}_i^\dagger & -v_+^{\dagger-1} v_-^\dagger \\ 1 & 0 \end{pmatrix}, \quad M_i \equiv \begin{pmatrix} -v_-^{-1} \tilde{h}_i & -v_-^{-1} v_+ \\ 1 & 0 \end{pmatrix}. \quad (31)$$

Notably, M_i and M'_i are the transfer matrices of the right-upper part h and left-lower part h^\dagger of the Hamiltonian \mathcal{H} in Eq. (27), respectively. In the canonical basis of Eqs. (27) and (29), h and $h' = h^\dagger$ are decomposed into the layer structure along the μ direction,

$$h_{i,j} = \tilde{h}_i \delta_{i,j} + v_+ \delta_{i,j-1} + v_- \delta_{i,j+1},$$

$$h'_{i,j} = \tilde{h}_i^\dagger \delta_{i,j} + v_-^\dagger \delta_{i,j-1} + v_+^\dagger \delta_{i,j+1},$$

where $i, j = 1, \dots, L_\mu$ are the indices of layers. From Eqs. (24) and (25), we obtain M_i of h and M'_i of h' as in Eq. (31). Note that M'_i is equivalent to $(M_i^\dagger)^{-1}$ under a certain transformation,

$$S \equiv \begin{pmatrix} 0 & -v_-^\dagger \\ v_+^\dagger & 0 \end{pmatrix}, \quad S M'_i S^{-1} = (M_i^\dagger)^{-1} = \begin{pmatrix} 0 & -v_-^\dagger v_+^{\dagger-1} \\ 1 & -\tilde{h}_i^\dagger v_+^{\dagger-1} \end{pmatrix}. \quad (32)$$

Thus, the LEs obtained by the product of $S M'_i S^{-1}$ have signs opposite to the LEs obtained by the product of M_i . The non-singular similarity transformation S does not change LEs. Thereby, the LEs of h and the LEs of $h' = h^\dagger$ come in opposite-sign pairs. The LEs of \mathcal{H} are the sum of the LEs of h and the LEs of h' .

2. Transfer matrix of the nodal-line semimetal model

The Hamiltonian of the nodal-line semimetal model reads

$$\mathcal{H} = \sum_{\mathbf{r}=(r_x, r_y, r_z)} \left\{ (\Delta + \epsilon_{\mathbf{r}}) c_{\mathbf{r}}^\dagger \sigma_z c_{\mathbf{r}} + \left[\sum_{\mu=x,y} \left(t_\perp c_{\mathbf{r}+\mathbf{e}_\mu}^\dagger \sigma_z c_{\mathbf{r}} \right) - i t_\parallel c_{\mathbf{r}+\mathbf{e}_z}^\dagger \sigma_y c_{\mathbf{r}} + t'_\parallel c_{\mathbf{r}+\mathbf{e}_z}^\dagger \sigma_z c_{\mathbf{r}} + \text{H.c.} \right] \right\}, \quad (33)$$

where $c_{\mathbf{r}}$ is a two-component annihilation operator on the cubic lattice site \mathbf{r} , σ_μ ($\mu = x, y, z$) are the Pauli matrices, Δ , t_\perp , t_\parallel , and t'_\parallel are real-valued parameters, $\epsilon_{\mathbf{r}}$ is a random potential that distributes uniformly in $[-W/2, W/2]$, and $\mathbf{e}_x = (1, 0, 0)$, $\mathbf{e}_y = (0, 1, 0)$, and $\mathbf{e}_z = (0, 0, 1)$ are the unit vectors. Note that the Hamiltonian in Eq. (33) reduces to Eq. (5) in the main text for $\Delta = 0$. Depending on Δ and the other parameters, Eq. (33) describes an ordinary insulator, topological insulator, and nodal-line semimetal [see Eq. (58)]. \mathcal{H} satisfies time-reversal symmetry $\mathcal{H} = \mathcal{H}^*$ and chiral symmetry $\mathcal{H} = -\mathcal{C}^\dagger \mathcal{H} \mathcal{C}$ with a unitary operator $\mathcal{C}_{\mathbf{r}, \mathbf{r}'} = \delta_{\mathbf{r}, \mathbf{r}'} \sigma_x$ with $\mathcal{C}^* = \mathcal{C}$, and thus belongs to the chiral orthogonal class (class BDI).

The chiral operator \mathcal{C} has eigenvalues $+1$ and -1 . Since \mathcal{C} is diagonal with respect to the lattice site, eigenvectors of \mathcal{C} can be labelled by the cubic-lattice site $\mathbf{s} \equiv (s_x, s_y, s_z)$:

$$\langle \mathbf{r} | v_{\mathbf{s}} \rangle = \delta_{\mathbf{r}, \mathbf{s}} \frac{1}{\sqrt{2}} \begin{pmatrix} 1 \\ 1 \end{pmatrix}, \quad \langle \mathbf{r} | u_{\mathbf{s}} \rangle = \delta_{\mathbf{r}, \mathbf{s}} \frac{1}{\sqrt{2}} \begin{pmatrix} 1 \\ -1 \end{pmatrix}, \quad (34)$$

satisfying $\mathcal{C}|v_s\rangle = |v_s\rangle$ and $\mathcal{C}|u_s\rangle = -|u_s\rangle$. Following Eq. (28), we construct the right-upper part h of \mathcal{H} on the same cubic lattice as,

$$(h)_{s,s} = \langle v_s | \mathcal{H} | u_s \rangle = \Delta + \epsilon_s, \quad (35)$$

$$(h)_{s+s+e_\mu,s} = (h)_{s,s+s+e_\mu} = \langle v_{s+s+e_\mu} | \mathcal{H} | u_s \rangle = \langle v_s | \mathcal{H} | u_{s+s+e_\mu} \rangle = t_\perp, \quad (36)$$

$$(h)_{s+s+e_z,s} = \langle v_{s+s+e_z} | \mathcal{H} | u_s \rangle = t_\parallel + t'_\parallel, \quad (37)$$

$$(h)_{s,s+s+e_z} = \langle v_s | \mathcal{H} | u_{s+s+e_z} \rangle = -t_\parallel + t'_\parallel, \quad (38)$$

for $\mu = x, y$. All the other matrix elements of h are zero. Notably, h can be regarded as a single-orbital tight-binding model,

$$h = \sum_{\mathbf{r}=(r_x,r_y,r_z)} \left[(\Delta + \epsilon_r) f_{\mathbf{r}}^\dagger f_{\mathbf{r}} + \sum_{\mu=x,y} \left(t_\perp f_{\mathbf{r}+e_\mu}^\dagger f_{\mathbf{r}} + \text{H.c.} \right) + (t'_\parallel + t_\parallel) f_{\mathbf{r}+e_z}^\dagger f_{\mathbf{r}} + (t'_\parallel - t_\parallel) f_{\mathbf{r}}^\dagger f_{\mathbf{r}+e_z} \right], \quad (39)$$

where $f_{\mathbf{r}}$ and $f_{\mathbf{r}}^\dagger$ are annihilation and creation operators at site \mathbf{r} . While h respects $h = h^*$, we have $h \neq h^\dagger$ for $t_\parallel \neq 0$. Hence, h generally belongs to the non-Hermitian symmetry class AI [33, 80].

The transfer matrix of h along the z direction is given by

$$M_i = \begin{pmatrix} -\frac{1}{t'_\parallel - t_\parallel} \tilde{h}_i & -\frac{t'_\parallel + t_\parallel}{t'_\parallel - t_\parallel} 1_{m \times m} \\ 1_{m \times m} & 0_{m \times m} \end{pmatrix}, \quad (40)$$

where $m = L^2$ is the degrees of freedom in each layer and the quasi-1D geometry ($L \times L \times L_z$, $L_z \gg L$) is considered. \tilde{h}_i is the Hamiltonian within the i th layer, which has $\Delta + \epsilon_s$ in its diagonal elements and t_\perp in its nearest-neighbor hopping.

For $t'_\parallel - t_\parallel = 0$, M_i is singular, and m eigenvalues of $\frac{1}{L_z} \ln M \equiv \frac{1}{L_z} \ln(M_{L_z} M_{L_z-1} \cdots M_1)$ diverge to ∞ . In fact, M_i^{-1} has zero eigenvalues with multiplicity m for $t'_\parallel = t_\parallel$,

$$M_i^{-1} = \begin{pmatrix} 0_{m \times m} & 1_{m \times m} \\ -\frac{t'_\parallel - t_\parallel}{t'_\parallel + t_\parallel} 1_{m \times m} & -\frac{1}{t'_\parallel + t_\parallel} \tilde{h}_i \end{pmatrix} \rightarrow \begin{pmatrix} 0_{m \times m} & 1_{m \times m} \\ 0_{m \times m} & -\frac{1}{t'_\parallel + t_\parallel} \tilde{h}_i \end{pmatrix} \quad (t'_\parallel - t_\parallel \rightarrow 0), \quad (41)$$

where $M^{-1} = M_1^{-1} \cdots M_{L_z-1}^{-1} M_{L_z}^{-1}$ has zero eigenvalue with multiplicity at least m . Therefore, m eigenvalues of $\frac{1}{2L_z} \ln(M^{-1})^\dagger M^{-1}$ always diverge to $-\infty$, while m eigenvalues of $\frac{1}{2L_z} \ln M^\dagger M$ always diverge to $+\infty$. The other m finite-valued LEs of h are determined from the following product:

$$\begin{aligned} p &\equiv - \lim_{L_z \rightarrow \infty} \frac{1}{2L_z} \ln \left(\frac{1}{t'_\parallel + t_\parallel} \tilde{h}_1 \cdots \frac{1}{t'_\parallel + t_\parallel} \tilde{h}_{L_z} \frac{1}{t'_\parallel + t_\parallel} \tilde{h}_{L_z}^\dagger \cdots \frac{1}{t'_\parallel + t_\parallel} \tilde{h}_1^\dagger \right), \\ &= \lim_{L_z \rightarrow \infty} \frac{1}{2L_z} \ln \left((t'_\parallel + t_\parallel) \tilde{h}_1^{-1\dagger} \cdots (t'_\parallel + t_\parallel) \tilde{h}_{L_z}^{-1\dagger} (t'_\parallel + t_\parallel) \tilde{h}_{L_z}^{-1} \cdots (t'_\parallel + t_\parallel) \tilde{h}_1^{-1} \right). \end{aligned} \quad (42)$$

E. Weak topological indices and Lyapunov exponents

We summarize a relationship between the weak topological indices of chiral-symmetric Hamiltonians and the numbers of positive and negative LEs of its right-upper part h in the canonical basis in Eq. (27) [66]. Consider a chiral-symmetric Hamiltonian $\mathcal{H}(\phi)$, in which a magnetic flux ϕ is inserted through a closed loop along the μ direction. Similarly to \mathcal{H} in Eq. (27), $\mathcal{H}(\phi)$ takes a block off-diagonal structure in a basis where the chiral operator is diagonal,

$$\mathcal{H}(\phi) = \begin{pmatrix} 0 & h(\phi) \\ h(\phi)^\dagger & 0 \end{pmatrix}. \quad (43)$$

The right-upper block $h(\phi)$ is decomposed into a layer structure along the μ direction,

$$h(\phi) = \begin{pmatrix} \tilde{h}_1 & v_- & 0 & \cdots & 0 & \frac{1}{z} v_+ \\ v_+ & \tilde{h}_2 & v_- & \cdots & \cdots & 0 \\ 0 & v_+ & \tilde{h}_3 & v_- & \cdots & 0 \\ \vdots & \vdots & \ddots & \ddots & \ddots & \vdots \\ zv_- & 0 & \cdots & 0 & v_+ & \tilde{h}_{L_\mu} \end{pmatrix}, \quad (44)$$

with $z = e^{i\phi}$. We assume that the hopping appears only between the nearest neighboring layers or within each layer. In the presence of next-nearest neighbor hopping, we can redefine two neighboring layers as one layer. v_- , v_+ , and $\tilde{h}_i (i = 1, 2, \dots, L_\mu)$ are $m \times m$ matrices, where m is the degrees of freedom of h in each layer. The 1D winding number w_μ along the μ direction is defined in terms of $h(\phi)$,

$$w_\mu \equiv i \int_0^{2\pi} \frac{d\phi}{2\pi} \partial_\phi \text{Tr} [\log [h(\phi)]] . \quad (45)$$

The winding number w_μ is given by the contour integral

$$\begin{aligned} w_\mu &= i \oint_{|z|=1} \frac{dz}{2\pi} \partial_z \text{Tr} [\log [h(z)]] \\ &= i \oint_{|z|=1} \frac{dz}{2\pi} \partial_z \log [\det [h(z)]] . \end{aligned} \quad (46)$$

Here, $\det [h(z)]$ is a polynomial function in terms of z with the lowest order z^{-m} and the highest order z^m if we have $\det v_- \neq 0$ and $\det v_+ \neq 0$. For simplicity, we assume $\det v_- \neq 0$ and $\det v_+ \neq 0$ while the following argument can be generalized to other cases. Then, $z^m \det [h(z)]$ is an analytic function of z , and w_μ is related to the number of zeros of $z^m \det [h(z)]$ within the circle $|z| = 1$,

$$\begin{aligned} w_\mu &= i \oint_{|z|=1} \frac{dz}{2\pi} \partial_z \log [z^{-m} z^m \det [h(z)]] \\ &= m + i \oint_{|z|=1} \frac{dz}{2\pi} \partial_z \log [z^m \det [h(z)]] \\ &= m + i \oint_{|z|=1} \frac{dz}{2\pi} \frac{\partial_z [z^m \det [h(z)]]}{z^m \det [h(z)]} \\ &= m - Z, \end{aligned} \quad (47)$$

where Z is the weighted number of the zeros, and the residue theorem is used in the last equality. $z = 0$ should not be a zero of $z^m \det [h(z)]$, since the lowest order of $\det [h(z)]$ is z^{-m} . Thus, Z is equal to the weighted number of the zeros of $\det [h(z)]$ in the disk $|z| < 1$.

The number of the zeros of $\det [h(z)]$ is determined by the LEs of h along the μ direction. For $\det [h(z)] = 0$, $h(z)$ has a zero mode. The presence of the zero modes is given by the transfer matrices of $h(z)$ along the μ direction. The transfer matrices for each layer are given by,

$$M_i(z) = \begin{cases} \begin{pmatrix} -v_-^{-1} \tilde{h}_1 & -\frac{1}{z} v_-^{-1} v_+ \\ 1 & 0 \end{pmatrix} & (i = 1), \\ \begin{pmatrix} -v_-^{-1} \tilde{h}_i & -v_-^{-1} v_+ \\ 1 & 0 \end{pmatrix} = M_i & (i = 2, 3, \dots, L_\mu - 1), \\ \begin{pmatrix} -\frac{1}{z} v_-^{-1} \tilde{h}_{L_\mu} & -\frac{1}{z} v_-^{-1} v_+ \\ 1 & 0 \end{pmatrix} & (i = L_\mu). \end{cases} \quad (48)$$

Here, $M_1(z)$ and $M_{L_\mu}(z)$ satisfy

$$M_1(z) M_{L_\mu}(z) = \begin{pmatrix} \frac{1}{z} v_-^{-1} \tilde{h}_1 v_-^{-1} \tilde{h}_{L_\mu} - \frac{1}{z} v_-^{-1} v_+ & \frac{1}{z} v_-^{-1} \tilde{h}_1 v_-^{-1} v_+ \\ -\frac{1}{z} v_-^{-1} \tilde{h}_{L_\mu} & -\frac{1}{z} v_-^{-1} v_+ \end{pmatrix} = \frac{1}{z} M_1(z=1) M_{L_\mu}(z=1) . \quad (49)$$

Suppose that $(A_1, A_2, \dots, A_{L_\mu})^T$ is a zero mode of $h(z)$ under the periodic boundary conditions. Then, we have

$$\begin{pmatrix} A_2 \\ A_1 \end{pmatrix} = M_1(z) \begin{pmatrix} A_1 \\ A_{L_\mu} \end{pmatrix}, \quad \begin{pmatrix} A_3 \\ A_2 \end{pmatrix} = M_2 \begin{pmatrix} A_2 \\ A_1 \end{pmatrix}, \quad \dots, \quad \begin{pmatrix} A_1 \\ A_{L_\mu} \end{pmatrix} = M_{L_\mu}(z) \begin{pmatrix} A_{L_\mu} \\ A_{L_\mu-1} \end{pmatrix}, \quad (50)$$

and hence

$$\begin{pmatrix} A_{L_\mu} \\ A_{L_\mu-1} \end{pmatrix} = M_{L_\mu-1} \dots M_2 M_1(z) M_{L_\mu}(z) \begin{pmatrix} A_{L_\mu} \\ A_{L_\mu-1} \end{pmatrix} \equiv \frac{1}{z} M \begin{pmatrix} A_{L_\mu} \\ A_{L_\mu-1} \end{pmatrix}, \quad (51)$$

where $M \equiv M_{L_\mu-1} \cdots M_2 M_1(z=1) M_{L_\mu}(z=1)$ is the product of the transfer matrices without the magnetic flux ($\phi=0$, $z=1$). Since $M_1(z=1)$ and $M_{L_\mu}(z=1)$ are statistically equivalent to $M_{L_\mu-1}$, $M_{L_\mu-2}$, \dots , M_3 , and M_2 , the eigenvalues of $\frac{1}{L_\mu} \ln M$ in the limit $L_\mu \rightarrow \infty$ are characterized by the LEs of h .

If $h(z)$ has a zero mode for a complex value z , M has an eigenvalue of z from Eq. (51), and vice versa. Thus, the number Z of the zeros of $\det[h(z)]$ within the disk $|z| < 1$ is equivalent to the number of eigenvalues of M whose absolute values are smaller than 1. The product M of L_μ random matrices has eigenvalues $e^{\alpha_j + i\beta_j}$ ($j = 1, 2, \dots, 2m; \alpha_j, \beta_j \in \mathbb{R}$), and generally, α_j grows linearly with L_μ , satisfying

$$\gamma_j = \lim_{L_\mu \rightarrow \infty} \frac{\alpha_j}{L_\mu}, \quad (52)$$

with the LE γ_j of M [66, 79, 81]. Thus, Z is also the same as the number N_- of the negative LEs of h :

$$Z = N_-. \quad (53)$$

In terms of Eq. (47), the 1D winding number is given by

$$w_\mu = m - N_- = \frac{1}{2}(N_+ - N_-), \quad (54)$$

where N_+ and N_- are the numbers of positive and negative LEs, satisfying $N_+ + N_- = 2m$. The weak topological index along the μ direction is the 1D winding number normalized by the degrees of freedom of h in each layer,

$$\nu_\mu = \frac{1}{m} w_\mu = \frac{1}{2m} (N_+ - N_-). \quad (55)$$

Notably, if a LE is exactly zero, the localization length ξ_μ along the μ direction diverges and the winding number w_μ is ill defined. In the quasi-1D geometry of a 3D disordered Hamiltonian ($L \times L \times L_\mu$, $L_\mu \gg L$), L^2 LEs are distributed within a finite range and form a continuous spectrum in the thermodynamic limit $L \rightarrow \infty$. When the spectrum crosses zero with changing W , w_μ also changes from an integer to another integer, ν_μ continuously changes with W , and the localization length always diverges.

1. Winding number in the clean limit

When a d -dimensional system has translation invariance in all the d -dimensional coordinates, Eq. (45) reduces to

$$w_\mu = i \int_0^{2\pi} \frac{dk_\mu}{2\pi} \partial_{k_\mu} \text{Tr} [\log [h(\mathbf{k})]], \quad (56)$$

with the momentum $\mathbf{k} \equiv (k_1, k_2, \dots, k_{d-1}, k_d)$ and the Bloch Hamiltonian $h(\mathbf{k})$. The trace includes the sum over momenta along the directions complementary to the μ direction. For example, the Bloch Hamiltonian for the 3D nodal-line semimetal model is given by the two-by-two matrix

$$\mathcal{H}(\mathbf{k}) = [\Delta + 2t_\perp (\cos k_x + \cos k_y) + 2t'_\parallel \cos k_z] \sigma_z - 2t_\parallel \sin k_z \sigma_y. \quad (57)$$

In the canonical basis where the chiral operator is diagonal, the matrix takes the block off-diagonal structure with

$$h(\mathbf{k}) = 2it_\parallel \sin k_z - [\Delta + 2t_\perp (\cos k_x + \cos k_y) + 2t'_\parallel \cos k_z]. \quad (58)$$

The complex number $h(\mathbf{k})$ winds around zero when k_z changes from 0 to 2π . For $|\Delta + 2t_\perp (\cos k_x + \cos k_y)| > 2|t'_\parallel|$, \mathcal{H} has an energy gap around $E=0$ and $h(\mathbf{k})$ winds around zero clockwise for all k_x and k_y in the first Brillouin zone, leading to $w_z = L^2$ and $\nu_z = 1$. Here, L^2 is the system size within the xy plane. For $|\Delta + 2t_\perp (\cos k_x + \cos k_y)| < 2|t'_\parallel|$, \mathcal{H} has a gap at $E=0$, but $h(\mathbf{k})$ does not wind around zero for any k_x and k_y , leading to $w_z = \nu_z = 0$. For $2|t'_\parallel| - 4t_\perp < \Delta < 2|t'_\parallel| + 4t_\perp$, zero modes of \mathcal{H} form a nodal ring in momentum space, and the winding number is +1 (0) for the wave numbers k_x, k_y inside (outside) the nodal ring, leading to $0 < \nu_z < 1$.

F. Statistical symmetry

An ensemble of disordered Hamiltonians, as a whole, can be invariant under a symmetry operation even if each disorder realization in the ensemble breaks the symmetry. Such symmetry of the ensemble is dubbed statistical symmetry [82]. Statistical symmetry does not influence the symmetry class of the Hamiltonians since it is not a symmetry of each disordered Hamiltonian. An example of statistical symmetry is translation symmetry in 3D weak topological insulators with disorder [83].

Statistical symmetry can make the ensemble averages of physical observables or topological indices be zero. A prime example is zero Hall conductance due to statistical time-reversal symmetry. Suppose that \mathcal{H}_α is a time-reversal-breaking Hamiltonian in an ensemble with statistical time-reversal symmetry and has a finite Hall conductance σ_{xy}^α . A time-reversed counterpart $\mathcal{H}_{\bar{\alpha}}$ of \mathcal{H}_α exists in the same ensemble and has the opposite value $-\sigma_{xy}^\alpha$ of the Hall conductance. Such an ensemble has zero Hall conductance on average,

$$\langle \sigma_{xy} \rangle = \frac{1}{2N_{\text{sample}}} \sum_{\alpha} (\sigma_{xy}^\alpha - \sigma_{xy}^\alpha) = 0. \quad (59)$$

1. Statistical symmetry, Lyapunov exponents, and one-dimensional winding number

In Sec. IE, the 1D winding numbers and weak topological indices are defined in terms of the right-upper part h of the chiral-symmetric Hamiltonian \mathcal{H} in the canonical basis [see Eq. (27)]. Now, we introduce statistical symmetry of h and show that it requires LEs of h to come in opposite-sign pairs. Statistical symmetry also makes the 1D winding numbers and weak topological indices be zero as a whole. Suppose that an ensemble of h with different disorder realizations, $\{h \mid \epsilon_{\mathbf{r}} \in [-W/2, W/2]\}$, is symmetric under transposition of h together with a certain unitary transformation \mathcal{U} :

$$\left\{ h \mid \epsilon_{\mathbf{r}} \in [-W/2, W/2] \right\} = \left\{ h' \mid \epsilon_{\mathbf{r}} \in [-W/2, W/2] \right\}, \quad \text{with} \quad h' \equiv \mathcal{U} h^T \mathcal{U}^\dagger. \quad (60)$$

Here, we assume that the unitary transformation \mathcal{U} is diagonal in a spatial coordinate r_μ and is independent of r_μ while it can be non-diagonal in the other coordinates \mathbf{s} ,

$$(\mathcal{U})_{\mathbf{r}, \mathbf{r}'} = \delta_{r_\mu, r'_\mu}(u)_{\mathbf{s}, \mathbf{s}'}, \quad (61)$$

with $\mathbf{r} \equiv (\mathbf{s}, r_\mu)$ and $\mathbf{r}' \equiv (\mathbf{s}', r'_\mu)$. Then, LEs of h along the μ direction come in opposite-sign pairs. The 1D winding number and weak topological index of h along the μ direction vanish from Eqs. (54) and (55).

To see this, we decompose h into a layer structure along the μ direction,

$$(h)_{i,j} = \tilde{h}_i \delta_{i,j} + v_+ \delta_{i,j-1} + v_- \delta_{i,j+1}, \quad (62)$$

with $i, j = 1, \dots, L_\mu$. \tilde{h}_i is a block of matrix elements of h within the i th layer, and v_\pm is a block of matrix elements of h between the i th layer and $(i \mp 1)$ th layer. v_\pm are free from disorder and independent of the layer index. If the degree of freedom in each layer of h is m , \tilde{h}_i and v_\pm are $m \times m$ matrices. Similarly, $h' \equiv \mathcal{U} h^T \mathcal{U}^\dagger$ is also decomposed into a layer structure along the μ direction,

$$(h')_{i,j} = u \tilde{h}_i^T u^\dagger \delta_{i,j} + u v_-^T u^\dagger \delta_{i,j-1} + u v_+^T u^\dagger \delta_{i,j+1}. \quad (63)$$

From Eqs. (24) and (25), the transfer matrices of h and h' are obtained as

$$M_i = \begin{pmatrix} -(v_-)^{-1} \tilde{h}_i & -(v_-)^{-1} v_+ \\ 1 & 0 \end{pmatrix}, \quad M'_i = \begin{pmatrix} -u(v_+^T)^{-1} \tilde{h}_i^T u^\dagger & -u(v_+^T)^{-1} v_-^T u^\dagger \\ 1 & 0 \end{pmatrix}. \quad (64)$$

The two matrices are related to each other by the following symmetry,

$$S M_i'^T S^{-1} = M_i^{-1}, \quad (65)$$

with

$$S \equiv \begin{pmatrix} 0 & -(v_-)^{-1} u^T \\ (v_+)^{-1} u^T & 0 \end{pmatrix}. \quad (66)$$

Since u and v_{\pm} in S are independent of the layer index, the same symmetry holds between the products of the transfer matrices, $M \equiv M_{L_{\mu}} \cdots M_1$ and $M' \equiv M'_{L_{\mu}} \cdots M'_1$,

$$SM'^T S^{-1} = M^{-1}. \quad (67)$$

Since a non-singular similarity transformation S does not change LEs, eigenvalues of $P'(0) \equiv \lim_{L_{\mu} \rightarrow \infty} \frac{1}{2L_{\mu}} \ln(M'^{\dagger} M')$ are opposite to eigenvalues of $P(0) \equiv \lim_{L_{\mu} \rightarrow \infty} \frac{1}{2L_{\mu}} \ln(M^{\dagger} M)$. Since h and h' are in the same ensemble, M_i and M'_j ($i, j = 1, \dots, L_{\mu}$) are random matrices with the same possibility distribution. Thus, according to Oseledec's theorem [79], the eigenvalues of $P(0)$ and $P'(0)$ converge to the same values in the limit $L_{\mu} \rightarrow \infty$. Then, the eigenvalues of $P(0)$, as well as the LEs of h , must come in opposite-sign pairs in the limit $L_{\mu} \rightarrow \infty$. Because of $N_+ = N_-$ for the LEs along the μ direction, ν_{μ} and w_{μ} of h vanish from Eqs. (54) and (55).

As discussed in Sec. ID, the LEs of h and the LEs of h^{\dagger} generally come in opposite-sign pairs. Thus, statistical Hermitian-conjugation symmetry of h also requires the LEs of h to come in the opposite-sign pairs. Suppose that an ensemble of h with different disorder realizations, $\{h | \epsilon_{\mathbf{r}} \in [-W/2, W/2]\}$, is symmetric under Hermitian conjugation together with a certain unitary transformation \mathcal{U} defined in Eq. (61):

$$\left\{ h \middle| \epsilon_{\mathbf{r}} \in [-W/2, W/2] \right\} = \left\{ h' \middle| \epsilon_{\mathbf{r}} \in [-W/2, W/2] \right\}, \quad \text{with} \quad h' \equiv \mathcal{U} h^{\dagger} \mathcal{U}^{\dagger}. \quad (68)$$

Then, the LEs of h along the μ direction should come in opposite-sign pairs, leading to $\nu_{\mu} = w_{\mu} = 0$.

It is also notable that statistical symmetry of h leads to statistical symmetry of \mathcal{H} . If an ensemble of h is invariant under the combination of transposition and a unitary operation in Eq. (60), the corresponding ensemble of \mathcal{H} is invariant under the combination of time reversal and a unitary operation:

$$\left\{ \mathcal{H} = \begin{pmatrix} 0 & h \\ h^{\dagger} & 0 \end{pmatrix} \middle| \epsilon_{\mathbf{r}} \in [-W/2, W/2] \right\} = \left\{ \mathcal{H}' = \begin{pmatrix} 0 & h' \\ h'^{\dagger} & 0 \end{pmatrix} \middle| \epsilon_{\mathbf{r}} \in [-W/2, W/2] \right\}, \quad \mathcal{H}' \equiv \begin{pmatrix} 0 & \mathcal{U} \\ \mathcal{U} & 0 \end{pmatrix} \mathcal{H}^* \begin{pmatrix} 0 & \mathcal{U}^{\dagger} \\ \mathcal{U}^{\dagger} & 0 \end{pmatrix}. \quad (69)$$

If an ensemble of h is invariant under the combination of Hermitian conjugation and a unitary transformation in Eq. (68), the corresponding ensemble of \mathcal{H} is invariant under the following unitary operation:

$$\left\{ \mathcal{H} = \begin{pmatrix} 0 & h \\ h^{\dagger} & 0 \end{pmatrix} \middle| \epsilon_{\mathbf{r}} \in [-W/2, W/2] \right\} = \left\{ \mathcal{H}' = \begin{pmatrix} 0 & h' \\ h'^{\dagger} & 0 \end{pmatrix} \middle| \epsilon_{\mathbf{r}} \in [-W/2, W/2] \right\}, \quad \mathcal{H}' \equiv \begin{pmatrix} 0 & \mathcal{U} \\ \mathcal{U} & 0 \end{pmatrix} \mathcal{H} \begin{pmatrix} 0 & \mathcal{U}^{\dagger} \\ \mathcal{U}^{\dagger} & 0 \end{pmatrix}. \quad (70)$$

2. Statistical symmetry in the nodal-line semimetal model

We show that the 3D nodal-line semimetal model has statistical transposition symmetries for the $\mu = x, y$ directions. The nodal-line semimetal model takes a block off-diagonal structure in the canonical basis, where the upper-right part h is given by Eq. (39). Transposition of h exchanges $t'_{\parallel} + t_{\parallel}$ and $t'_{\parallel} - t_{\parallel}$ in Eq. (39). Since the disorder potential $\epsilon_{\mathbf{r}}$ is statistically equivalent for different lattice points \mathbf{r} , we can introduce a mirror operation with respect to the xy plane as a unitary transformation of Eqs. (60) and (61),

$$\mathcal{U}_{(r_x, r_y, r_z | r'_x, r'_y, r'_z)} = \delta_{r_x, r'_x} \delta_{r_y, r'_y} \delta_{r_z, -r'_z}. \quad (71)$$

This mirror operation exchanges $t'_{\parallel} + t_{\parallel}$ and $t'_{\parallel} - t_{\parallel}$ as well as ϵ_{r_x, r_y, r_z} and $\epsilon_{r_x, r_y, -r_z}$ while $\epsilon_{\mathbf{r}}$ is statistically equivalent for different \mathbf{r} . Thus, an ensemble for h defined by Eq. (39) is statistically invariant under transposition with the unitary transformation. The symmetry of Eqs. (60) and (71) requires the LEs of h along the x (y) direction to come in opposite-sign pairs, leading to $w_{x(y)} = \nu_{x(y)} = 0$.

G. Finite-size scaling of Lyapunov exponents

The LEs of a chiral-symmetric Hamiltonian \mathcal{H} are the sum of LEs of the right-upper part h of \mathcal{H} in the canonical basis and their opposite-sign exponents [see Eq. (27)]. In the quasi-one-dimensional (quasi-1D) geometry, the LEs of \mathcal{H} , as well as the LEs of h , comprise continuum spectra for the limit $L \rightarrow \infty$ [62]. In the nodal-line semimetal model \mathcal{H} with $t_{\parallel} = t'_{\parallel}$, $m = L^2$ LEs of diverge to $+\infty$, and the other m LEs of h form a finite spectrum around $\gamma = 0$ (see also Fig. 2 in the main text). For $t_{\parallel} \neq t'_{\parallel}$, on the other hand, all the $2m = 2L^2$ LEs of h comprise either one or two continuum spectra around $\gamma = 0$, depending on the disorder strength (see Figs. 9(c) and 9(d)).

In the following discussion, we focus on the case with the two continuum LE spectra. Generalization to the other cases is straightforward. For finite L , the transfer matrix study of the non-Hermitian Hamiltonian h in the quasi-1D geometry gives a discrete set of $2m$ LEs,

$$\{\gamma_{\min}^{(1)}(W, L), \dots, \gamma_{\max}^{(1)}(W, L), \gamma_{\min}^{(2)}(W, L), \dots, \gamma_{\max}^{(2)}(W, L)\}, \quad (72)$$

with $\gamma_{\min}^{(1)}(W, L) < \dots < \gamma_{\max}^{(1)}(W, L) < \gamma_{\min}^{(2)}(W, L) < \dots < \gamma_{\max}^{(2)}(W, L)$. In the limit $L \rightarrow \infty$, all the m LEs from $\gamma_{\min}^{(j)}(W, L)$ to $\gamma_{\max}^{(j)}(W, L)$ ($j = 1, 2$) form a continuum spectrum that ranges from $\gamma_{\min}^{(j)}(W)$ to $\gamma_{\max}^{(j)}(W)$, satisfying

$$\lim_{L \rightarrow \infty} \gamma_{\min}^{(j)}(W, L) \equiv \gamma_{\min}^{(j)}(W), \quad \lim_{L \rightarrow \infty} \gamma_{\max}^{(j)}(W, L) \equiv \gamma_{\max}^{(j)}(W), \quad (73)$$

with $j = 1, 2$. For some disorder strength, a finite gap $2\Delta \equiv \gamma_{\min}^{(2)}(W) - \gamma_{\max}^{(1)}(W)$ exists between the two continuum LEs spectra (see Figs. 7, 9(c), and 9(d)).

When the gap 2Δ is much larger than L^{-1} , $\gamma_{\max}^{(1)}(W, L)$ and $\gamma_{\min}^{(2)}(W, L)$ can be fitted well by the following scaling functions:

$$\gamma_{\max}^{(1)}(W, L) = -\frac{a}{L} + \gamma_{\max}^{(1)}(W). \quad (74)$$

and

$$\gamma_{\min}^{(2)}(W, L) = \frac{a}{L} + \gamma_{\min}^{(2)}(W), \quad (75)$$

Notably, this scaling holds irrespective of whether their limits $\gamma_{\min}^{(2)}(W)$ and $\gamma_{\max}^{(1)}(W)$ are close to zero. To see this, we first note that LEs of h with different t_{\parallel} and t'_{\parallel} are related by an imaginary gauge transformation along the z direction [68]. Let the imaginary gauge transformation with an imaginary gauge ig act on h by

$$h \rightarrow h_g \equiv V_g h V_g^{-1}, \quad (76)$$

where V_g is a diagonal matrix whose diagonal element takes e^{jg} in the j th layer along the z direction:

$$V_g = \begin{pmatrix} e^g 1_{m \times m} & 0 & 0 & \dots & 0 \\ 0 & e^{2g} 1_{m \times m} & 0 & \dots & 0 \\ \vdots & \vdots & \ddots & \vdots & \vdots \\ 0 & \dots & \dots & \dots & e^{Lzg} 1_{m \times m} \end{pmatrix}. \quad (77)$$

The transfer matrix $M_i(g)$ of $h_g \equiv V_g h V_g^{-1}$ along the z direction is obtained from Eq. (40) as

$$M_i(g) = \begin{pmatrix} -e^g \frac{1}{t'_{\parallel} - t_{\parallel}} \tilde{h}_i & -e^{2g} \frac{t'_{\parallel} + t_{\parallel}}{t'_{\parallel} - t_{\parallel}} 1_{m \times m} \\ 1_{m \times m} & 0_{m \times m} \end{pmatrix}, \quad (78)$$

and satisfies

$$M_i(g) = e^g S \begin{pmatrix} -\frac{1}{t'_{\parallel} - t_{\parallel}} \tilde{h}_i & -\frac{t'_{\parallel} + t_{\parallel}}{t'_{\parallel} - t_{\parallel}} 1_{m \times m} \\ 1_{m \times m} & 0_{m \times m} \end{pmatrix} S^{-1} = e^g S M_i S^{-1}, \quad S = \begin{pmatrix} 1_{m \times m} & 0_{m \times m} \\ 0_{m \times m} & e^{-g} 1_{m \times m} \end{pmatrix}. \quad (79)$$

Thus, the LEs of h_g are obtained from the LEs of h in Eq. (72),

$$\{\gamma_{\min}^{(1)}(W, L) + g, \dots, \gamma_{\max}^{(1)}(W, L) + g, \gamma_{\min}^{(2)}(W, L) + g, \dots, \gamma_{\max}^{(2)}(W, L) + g\}. \quad (80)$$

Similarly, the LEs of h_g^{\dagger} differ from the LEs of h^{\dagger} by $-g$. Suppose that the gap between $\gamma_{\max}^{(1)}(W)$ and $\gamma_{\min}^{(2)}(W)$ is much larger than L^{-1} , and choose the imaginary gauge g in such a way that a midpoint of the gap comes around zero,

$$\gamma_{\max}^{(1)}(W) + g < 0 < \gamma_{\min}^{(2)}(W) + g. \quad (81)$$

Then, a zero mode of a chiral-symmetric Hamiltonian \mathcal{H}_g that has h_g and h_g^\dagger in the off-diagonal blocks is in the Anderson insulator phase, and its localization length ξ_z is much shorter than L . Depending on g , the localization length is given by either

$$\frac{1}{\xi_z(W, L)} = -(\gamma_{\max}^{(1)}(W, L) + g), \quad (82)$$

or

$$\frac{1}{\xi_z(W, L)} = \gamma_{\min}^{(2)}(W, L) + g. \quad (83)$$

In the Anderson insulator phase, a finite-size scaling of the normalized localization length $\Lambda(L) \equiv \xi(L)/L$ is described by a function of the single parameter Λ (i.e., single-parameter scaling) [69]:

$$\frac{d \ln \Lambda}{d \ln L} = \beta(\Lambda). \quad (84)$$

For small Λ , we have $\beta(\Lambda) \rightarrow -1$ and $\ln \Lambda \simeq \ln \xi(L = \infty) - \ln L$. When the localization length ξ is much shorter than L , one may expand the β function in small Λ , $\beta(\Lambda) = -1 + a\Lambda + \mathcal{O}(\Lambda^2)$, and retain the zeroth and first order in Λ ,

$$\frac{d \ln \Lambda}{d \ln L} = -1 + a\Lambda. \quad (85)$$

This differential equation may be solved by an integration in a domain of $[L, L_0]$ with $L \ll L_0$,

$$\frac{L}{\xi} \equiv \frac{1}{\Lambda} = a + \frac{L}{L_0} \left(\frac{1}{\Lambda_0} - a \right) \equiv a + \frac{L}{L_0} \left(\frac{L_0}{\xi_0} - a \right), \quad (86)$$

with $\xi_0 \equiv \xi(L = L_0)$. When L_0 goes to infinity, ξ_0 converges to finite $\xi(L = \infty) \equiv \xi(\infty)$. Thus, we obtain the lowest-order finite-size scaling form of the quasi-1D localization length,

$$\frac{1}{\xi(L)} = \frac{a}{L} + \frac{1}{\xi(\infty)}. \quad (87)$$

Now that the localization length along the z direction is much shorter than L in Eqs. (82) and (83), we may use the same scaling function not only for $\xi_z(W, L)$ but also for $\gamma_{\min}^{(2)}(W, L)$ and $\gamma_{\max}^{(1)}(W, L)$. In fact, the scaling forms of Eqs. (74) and (75) work well for the numerical fittings. Note that the coefficient a in Eq. (87) takes a non-universal value in general (see the fitting values in Table VIII). To obtain the scaling form for $\gamma_{\min}^{(1)}(W, L)$, let us choose large positive g and make all the LEs of h_g be positive,

$$0 < \gamma_{\min}^{(1)}(W, L) + g. \quad (88)$$

In the chiral-symmetric Hamiltonian \mathcal{H}_g that has such h_g and its Hermitian conjugate h_g^\dagger , $E = 0$ is in the weak topological insulator phase ($\nu_z = 1$) and the localization length ξ_z is given by $\gamma_{\min}^{(1)}(W, L) + g$. If we assume that the finite-size scaling of ξ_z in the weak topological insulator phase is also described by the single parameter scaling function of $\Lambda_z \equiv \xi_z/L$, we also obtain the scaling function for $\gamma_{\min}^{(1)}(W, L)$ as

$$\gamma_{\min}^{(1)}(W, L) = \frac{a}{L} + \gamma_{\min}^{(1)}(W). \quad (89)$$

This scaling form also works well for the numerical data of $\gamma_{\min}^{(1)}(W, L)$.

1. Numerical fitting

To show the validity of the scaling forms in Eqs. (74) and (75), we use the standard χ^2 fitting method to fit the data of $\gamma_{\min/\max}^{(i)}(W, L)$ ($i = 1, 2$) with larger L . For fixed W , we minimize the following χ^2 function with respect to a and $\gamma_{\min/\max}^{(i)}(W)$ in Eqs. (74) and (75),

$$\chi^2 = \sum_{j=1}^D \left(\frac{F_j - \gamma_{\min/\max}^{(i)}(W, L)}{\sigma_j} \right)^2, \quad (90)$$

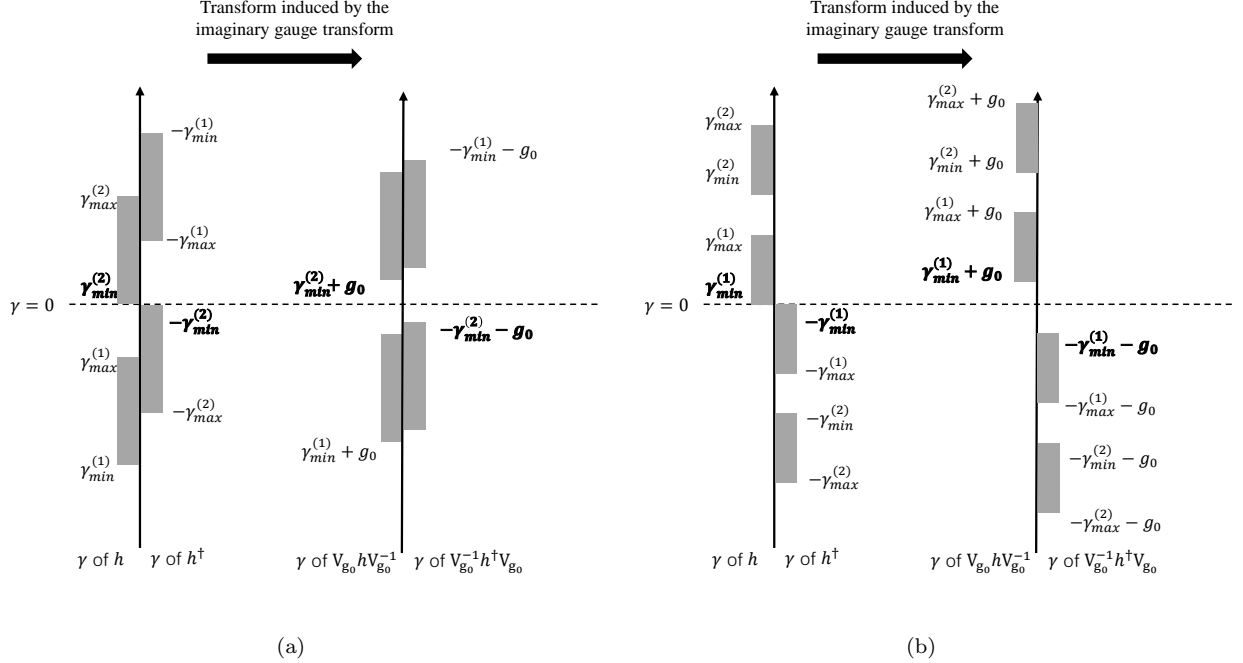


FIG. 4. Schematic pictures of Lyapunov exponents (LEs) of the nodal-line semimetal model \mathcal{H} and LEs of \mathcal{H}_g generated by an imaginary gauge transformation. The LEs of \mathcal{H} and \mathcal{H}_g are the sum of LEs of its right-upper non-Hermitian Hamiltonian h and their Hermitian conjugate h^\dagger in Eq. (27). The LEs calculated in the quasi-1D geometry ($L \times L \times L_z$, $L_z \gg L$) comprise two continuum LEs spectra in the limit $L \rightarrow \infty$. The grey-shaded regions in the left (right) sides of the vertical axis denote the continuous spectra formed by LEs of h (h^\dagger). The dotted horizontal line denotes zero $\gamma = 0$. The LEs of \mathcal{H} and \mathcal{H}_g , as a whole, are symmetric around zero. The smallest positive or the largest negative LE (marked in bold) corresponds to the inverse of the quasi-1D localization length. In (a), g is chosen such that finite $\gamma_{\min}^{(2)}(W) + g$ corresponds to the inverse of the localization length of \mathcal{H}_g . In (b), g is chosen such that $\gamma_{\min}^{(1)}(W) + g$ corresponds to the inverse of the localization length of \mathcal{H}_g .

where j specifies the data point of $\gamma_{\min/\max}^{(i)}(W, L)$ with different L . The number D of the data points is typically 7 ($14 \leq L \leq 28$) and 9 ($18 \leq L \leq 34$). F_j is the fitted value from Eqs. (74) and (75) for different L specified by j . σ_j is the standard deviation of $\gamma_{\min/\max}^{(i)}(W, L)$ estimated from the transfer matrix calculation [61]. The finite-size scaling fit works well in the nodal-line semimetal models with or without time-reversal symmetry that are studied in this work. Some fitting results for the nodal-line semimetal models ($\Delta = 0$, $t_{\parallel} = t'_{\parallel} = 1/2$, $t_{\perp} = 1$) that are studied in the main text are shown in Fig. 5 (a,c) and Table IV. In Table IV, the Monte Carlo method is used to generate pseudo-data sets and evaluate the 95% confidence interval of the fitted values of “ a ” and “ $\gamma_{\min/\max}^{(1)}(W)$ ”.

Using $\gamma_{\max}^{(1)}(W)$ with the confidence interval, we determine the critical disorder strength $W_c^{(z)}$ between the non-localized region and the localized phase. For example, the fitting results in Table IV show $\gamma_{\max} = 0.0020 [0.0017, 0.0022]$ for $W = 29.5$ and $\gamma_{\max} = -0.0042 [-0.0044, 0.0040]$ for $W = 29.4$ in the nodal-line semimetal model in symmetry class BDI. The results suggest that $W_c^{(z)}$ must be between 29.4 and 29.5 with the 95% confidence: $W_c^{(z)} = 29.45 [29.4, 29.5]$. $W_c^{(z)}$ for the nodal-line semimetal models in symmetry classes BDI and AIII are summarized in Table V. Table V also shows $W_c^{(x)}$ in the same nodal-line semimetal models for the same sets of parameters. Comparisons between $W_c^{(z)}$ and $W_c^{(x)}$ illustrate that $W_c^{(x)} < W_c^{(z)}$ and $|W_c^{(z)} - W_c^{(x)}|$ is around 10% of $W_c^{(x)}$. This concludes the presence of the quasi-localized phase in these nodal-line semimetal models. Similarly, comparisons of $W_c^{(z)}$ and $W_c^{(x)}$ in other types of nodal-line semimetal models (Tables VII and IX) also suggest the presence of the quasi-localized phases (see below).

TABLE IV. Finite-size scaling analysis of $\gamma_{\max}^{(1)}(W, L)$ for several disorder strength W around $W = W_c^{(z)}$ in the nodal-line semimetal models ($\Delta = 0$, $t_{\parallel} = t'_{\parallel} = 1/2$, $t_{\perp} = 1$) with time-reversal symmetry (symmetry class BDI) and without time-reversal symmetry (symmetry class AIII). The square brackets are the 95% confidence intervals determined by the Monte Carlo analyses.

symmetry class	W	L	$\gamma_{\max}(W, L = \infty)$	a	GOF
BDI	29.4	18 - 34	0.0020 [0.0017, 0.0022]	-3.890 [-3.893, -3.888]	0.58
BDI	29.5	18 - 34	-0.0042 [-0.0044, -0.0040]	-3.689 [3.691, -3.687]	0.14
AIII	9.70	14 - 28	0.0143 [0.0128, 0.0156]	-1.921 [-1.948, -1.892]	0.02
AIII	9.80	14 - 28	0.0015 [0.0000, 0.0029]	-1.929 [-1.957, -1.899]	0.50
AIII	9.90	14 - 28	-0.0114 [-0.0129, -0.0099]	-1.931 [-1.961, -1.904]	0.22

TABLE V. Comparison between the critical disorder strength $W_c^{(z)}$ in the z direction (weak topological index $\nu_z \neq 0$) and the critical disorder strength $W_c^{(x)}$ in the x direction (weak topological index $\nu_x = 0$) for the nodal-line semimetal models in symmetry classes BDI and AIII ($\Delta = 0$, $t_{\parallel} = t'_{\parallel} = 1/2$, $t_{\perp} = 1$). The square brackets denote the 95% intervals. The confidence intervals of $W_c^{(x)}$ are determined by the 95% confidence intervals of $\gamma_{\max}(W)$.

symmetry class	$W_c^{(x)}$	$W_c^{(z)}$
BDI	27.24[27.19, 27.30]	29.45[29.4, 29.5]
AIII	9.14[9.12, 9.17]	9.8[9.7, 9.9]

H. Quasi-localized phases in chiral-symmetric models with weak topological indices

In Sec. I G, we describe the finite-size scaling analysis of the LEs along the z direction in the nodal-line models with the weak topological index $\nu_z \neq 0$. The analysis enables determinations of the phase boundary $W_c^{(z)}$ of the non-localized region. The non-localized region comprises the metal and quasi-localized phases. In the nodal-line models with $\nu_x = \nu_y = 0$, the phase transition between the metal and quasi-localized phases is characterized by the localization properties along the x or y direction. In this section, we discuss the localization properties along the x direction in the chiral-symmetric models with $\nu_z \neq 0$ and $\nu_x = 0$. We demonstrate the presence of the quasi-localized phases inside the non-localized region for all the models.

1. Nodal-line semimetal in class AIII

We discuss a nodal-line semimetal in Eq. (33) with the time-reversal-breaking disorder. The Hamiltonian \mathcal{H}_1 has the two types of random potentials,

$$\mathcal{H}_1 = \sum_{\mathbf{r}=(r_x, r_y, r_z)} \left\{ (\Delta + \epsilon_{\mathbf{r}}) c_{\mathbf{r}}^{\dagger} \sigma_y c_{\mathbf{r}} + \epsilon'_{\mathbf{r}} c_{\mathbf{r}}^{\dagger} \sigma_z c_{\mathbf{r}} + \left[\sum_{\mu=x, y} \left(t_{\perp} c_{\mathbf{r}+\mathbf{e}_{\mu}}^{\dagger} \sigma_z c_{\mathbf{r}} \right) - i t_{\parallel} c_{\mathbf{r}+\mathbf{e}_z}^{\dagger} \sigma_y c_{\mathbf{r}} + t'_{\parallel} c_{\mathbf{r}+\mathbf{e}_z}^{\dagger} \sigma_z c_{\mathbf{r}} + \text{H.c.} \right] \right\}, \quad (91)$$

where the random potential $\epsilon_{\mathbf{r}}$ ($\epsilon'_{\mathbf{r}}$) respects (breaks) time-reversal symmetry and distributes uniformly in $\epsilon_{\mathbf{r}}^2 + \epsilon_{\mathbf{r}}'^2 \leq W^2$. The parameters are chosen to be $\Delta = 0$, $t_{\parallel} = t'_{\parallel} = 1/2$, and $t_{\perp} = 1$. The Hamiltonian \mathcal{H}_1 only satisfies chiral symmetry $\mathcal{H}_1 = -\sigma_x \mathcal{H}_1 \sigma_x$, and hence belongs to class AIII.

According to Eq. (28), the chiral-symmetric Hamiltonian is decomposed into the block-off diagonal structure in the basis that diagonalizes the chiral operator $\mathcal{C} \equiv \sigma_x$. The right-upper part h_1 of \mathcal{H}_1 in this basis is given by

$$h_1 = \sum_{\mathbf{r}=(r_x, r_y, r_z)} \left[(\Delta + \epsilon_{\mathbf{r}} + i\epsilon'_{\mathbf{r}}) f_{\mathbf{r}}^{\dagger} f_{\mathbf{r}} + \sum_{\mu=x, y} \left(t_{\perp} f_{\mathbf{r}+\mathbf{e}_{\mu}}^{\dagger} f_{\mathbf{r}} + \text{H.c.} \right) + (t'_{\parallel} + t_{\parallel}) f_{\mathbf{r}+\mathbf{e}_z}^{\dagger} f_{\mathbf{r}} + (t'_{\parallel} - t_{\parallel}) f_{\mathbf{r}}^{\dagger} f_{\mathbf{r}+\mathbf{e}_z} \right]. \quad (92)$$

Transposition exchanges $t'_{\parallel} + t_{\parallel}$ and $t'_{\parallel} - t_{\parallel}$. Thus, as a unitary transformation in Eqs. (60) and (61), we can consider the mirror operation with respect to the xy plane as in Eq. (71). Since both $\epsilon_{\mathbf{r}}$ and $\epsilon'_{\mathbf{r}}$ are statistically equivalent for different lattice points \mathbf{r} , an ensemble of h_1 defined in Eq. (92) is statistically invariant under the combination of

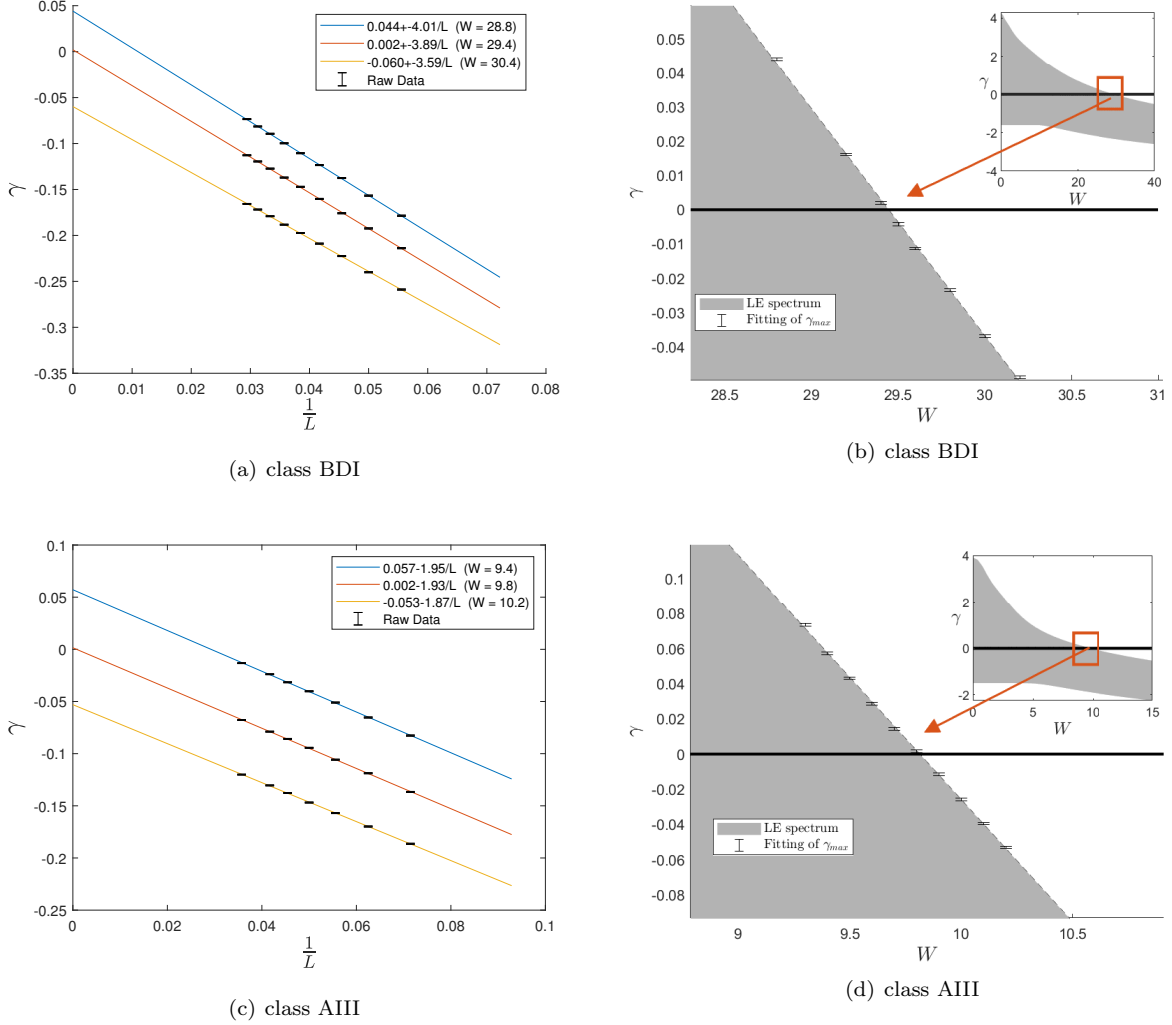


FIG. 5. (a,c) $\gamma_{\max}^{(1)}(W, L)$ as a function of the system size L for the different disorder strength W in the nodal-line semimetal models ($\Delta = 0$, $t_{\parallel} = t'_{\parallel} = 1/2$, $t_{\perp} = 1$) in (a) symmetry class BDI and (c) symmetry class AIII. The solid lines are the fitting curves from Eq. (75). A cross-section of the fitting curve at $1/L = 0$ determines $\gamma_{\max}^{(1)}(W) \equiv \lim_{L \rightarrow \infty} \gamma_{\max}^{(1)}(W, L)$. (b,d) $\gamma_{\max}^{(1)}(W)$ as a function of W around $W = W_c^{(z)}$ in the nodal-line semimetal models in (b) symmetry class BDI and (d) symmetry class AIII. Insets of (b,d): distributions of the Lyapunov exponents (LEs) of the right-upper part h of the nodal-line semimetal model \mathcal{H} as a function of W in the larger range of γ and W . The LEs of the nodal-line semimetal models are the sum of the LEs of h and their opposite-sign exponents.

transposition and the mirror operation. The symmetry in Eqs. (60) and (71) requires the LEs of h_1 along the x and y directions to come in opposite-sign pairs, leading to $\nu_x = \nu_y = 0$.

We calculate the localization length ξ_x of h_1 along the x direction in the quasi-1D geometry ($L_x \times L \times L$, $L_x \gg L$). The normalized localization length $\Lambda_x \equiv \xi_x/L$ shows scale-invariant behavior around $W_c^{(x)} = 9.14 \pm 0.01$ (Fig. 6). Fitting by the polynomial expansion of the finite-size scaling functions [see Eqs. (20) and (21)], we determine the critical disorder strength $W_c^{(x)}$ and the critical exponent (see Table III). Figure 6 shows the normalized localization length for different W and L together with the fitting curves.

In Sec. I G, we use the finite-size scaling of LEs to obtain the critical disorder strength $W_c^{(z)} = 9.8 [9.7, 9.9]$. For $W < W_c^{(z)}$, the localization length along the z direction diverges. $W_c^{(x)}$ is well within the non-localized region, $W_c^{(x)} < W_c^{(z)} = 9.8 [9.7, 9.9]$, demonstrating the presence of the quasi-localized phase in the nodal-line semimetal model without time-reversal symmetry.

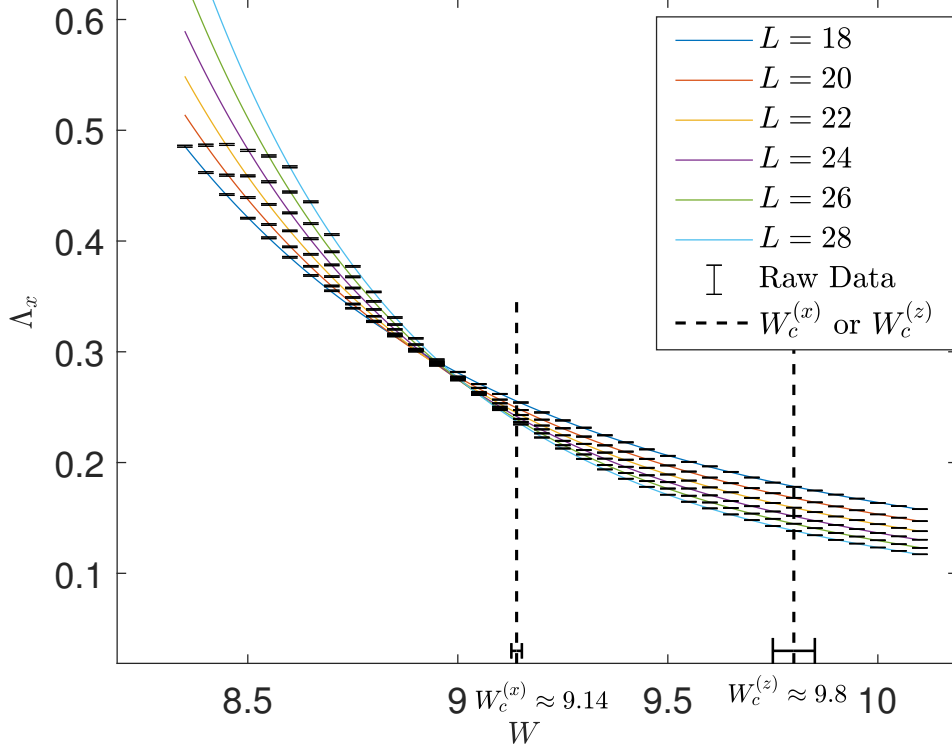


FIG. 6. Normalized localization length $\Lambda_x \equiv \xi_x/L$ along the x direction as a function of the disorder strength W in the nodal-line semimetal model in class AIII [Eq. (33) with $\Delta = 0$, $t_{\parallel} = t'_{\parallel} = 1/2$, $t_{\perp} = 1$]. ξ_x is calculated in the quasi-1D geometry ($L \times L \times L_x$). The black points are the raw data with the error bars. The solid lines for different L and the dashed vertical line $W_c^{(x)} \approx 9.14$ with the error bars are the results of the fitting according to Eqs. (20) and (21) with $(m, n) = (2, 3)$. The dashed line $W_c^{(z)} \approx 9.8$ is evaluated by the fitting of the Lyapunov exponents along the z direction by Eq. (74).

2. Nodal-line semimetals in class BDI

We also study the localization properties along the x direction in other nodal-line semimetal models in class BDI: i) nodal-line semimetal model in Eq. (33) with the different parameters $\Delta = 0$, $t_{\parallel} = \sinh g$, $t'_{\parallel} = \cosh g$ ($g = 0.22, 1$), $t_{\perp} = 1$ and ii) another nodal-line semimetal model \mathcal{H}_2 with an extended Fermi line running across the Brillouin zone,

$$\mathcal{H}_2 = \sum_{\mathbf{r}=(r_x, r_y, r_z)} \left\{ (\Delta + \epsilon_{\mathbf{r}}) c_{\mathbf{r}}^{\dagger} \sigma_z c_{\mathbf{r}} + \left[t_{\perp} c_{\mathbf{r}+\mathbf{e}_x}^{\dagger} \sigma_z c_{\mathbf{r}} + \sum_{\mu=y,z} \left(-it_{\parallel} c_{\mathbf{r}+\mathbf{e}_{\mu}}^{\dagger} \sigma_y c_{\mathbf{r}} + t'_{\parallel} c_{\mathbf{r}+\mathbf{e}_{\mu}}^{\dagger} \sigma_z c_{\mathbf{r}} \right) + \text{H.c.} \right] \right\}, \quad (93)$$

where $\epsilon_{\mathbf{r}}$ takes real values and distributes uniformly in $[-W/2, W/2]$, and the parameters are chosen to be $\Delta = 0$, $t_{\parallel} = \cosh g$, $t'_{\parallel} = \sinh g$ ($g = 0.2$), $t_{\perp} = 1$. The Hamiltonian \mathcal{H}_2 satisfies time-reversal symmetry $\mathcal{H}_2 = \mathcal{H}_2^*$ and chiral symmetry $\mathcal{H}_2 = -\sigma_x \mathcal{H}_2 \sigma_x$, and hence belongs to class BDI. In terms of Eq. (28), the chiral-symmetric Hamiltonian \mathcal{H}_2 is decomposed into the block-off diagonal structure in the canonical basis where σ_x is diagonalized. The right-upper part h_2 of \mathcal{H}_2 in this basis is given by

$$h_2 = \sum_{\mathbf{r}=(r_x, r_y, r_z)} \left\{ (\Delta + \epsilon_{\mathbf{r}}) f_{\mathbf{r}}^{\dagger} f_{\mathbf{r}} + \left(t_{\perp} f_{\mathbf{r}+\mathbf{e}_x}^{\dagger} f_{\mathbf{r}} + \text{H.c.} \right) + \sum_{\mu=y,z} \left[(t'_{\parallel} + t_{\parallel}) f_{\mathbf{r}+\mathbf{e}_{\mu}}^{\dagger} f_{\mathbf{r}} + (t'_{\parallel} - t_{\parallel}) f_{\mathbf{r}}^{\dagger} f_{\mathbf{r}+\mathbf{e}_{\mu}} \right] \right\}. \quad (94)$$

Transposition exchanges $t'_{\parallel} + t_{\parallel}$ and $t'_{\parallel} - t_{\parallel}$. Thus, as a unitary transformation in Eqs. (60) and (61), we can apply a π -rotation around the x axis,

$$\mathcal{U}_{(r_x, r_y, r_z | r'_x, r'_y, r'_z)} = \delta_{r_x, r'_x} \delta_{r_y, -r'_y} \delta_{r_z, -r'_z}. \quad (95)$$

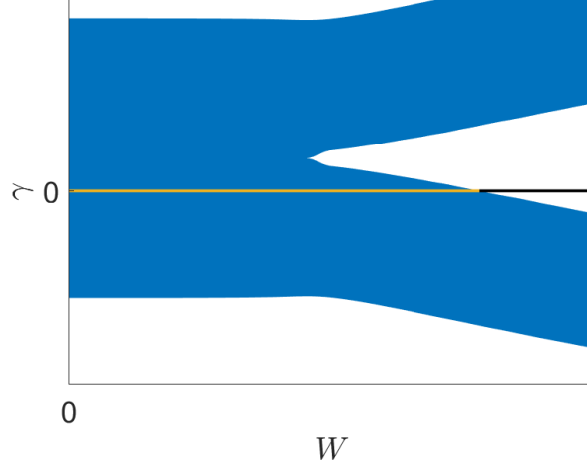


FIG. 7. $2L^2$ Lyapunov exponents (LEs) of the right-upper part h of the nodal-line semimetal model \mathcal{H} in the canonical basis ($t_{\perp} = 3/10, t'_{\parallel} = 1, t_{\parallel} = 1/4, \Delta = 2$) calculated along the z direction with the quasi-1D geometry $L \times L \times L_z$. Distributions of the $2L^2$ LEs are plotted as a function of the disorder strength W . The LEs of the nodal-line semimetal model are the sum of the $2L^2$ LEs of h and their opposite-sign exponents.

TABLE VI. Polynomial fitting results of the normalized localization length $\Lambda_x \equiv \xi_x/L$ in the x direction around its scaling invariant point of the different nodal-line semimetal models \mathcal{H} [Eq. (33)] and \mathcal{H}_2 [Eq. (93)]. Both models are characterized by the parameters $\Delta = 0$, $t_{\parallel} = \sinh g$, $t'_{\parallel} = \cosh g$, $t_{\perp} = 1$. The column “parameter” specifies the value of g . The data of Λ_x in these models are calculated with the quasi-1D geometry ($L \times L \times L_z$, $L_z \gg L$). The range of the system size L , critical disorder strength $W_c^{(x)}$, critical exponent ν , scaling dimension $-y$ of the least irrelevant variable, critical localization length Λ_c , the goodness of fitting (GOF), and the fitting order (m, n) in Eqs. (20) and (21) are shown. The square brackets are the 95% confidence error bars determined by the synthetic data. Note that Λ_c is non-universal because of the spatial anisotropy.

model	parameter	L	m	n	GOF	$W_c^{(x)}$	ν	y	Λ_c
\mathcal{H}	$g = 0.22$	20-34	2	3	0.61	21.688[21.647,21.729]	0.866[0.792,0.916]	1.840[1.608,2.130]	0.239[0.232,0.246]
\mathcal{H}	$g = 0.22$	20-34	3	3	0.58	21.730[21.662,21.803]	0.860[0.679,0.918]	1.619[1.284,2.031]	0.232[0.218,0.243]
\mathcal{H}	$g = 1$	18-28	2	3	0.14	41.284[41.209,41.365]	0.787[0.754,0.818]	2.256[2.013,2.516]	0.110[0.108,0.113]
\mathcal{H}	$g = 1$	18-28	3	3	0.24	41.358[41.264,41.463]	0.785[0.751,0.817]	2.088[1.816,2.381]	0.108[0.104,0.111]
\mathcal{H}_2	$g = 0.2$	20-28	2	3	0.32	23.214[23.146,23.334]	0.857[0.712,0.920]	2.595[1.845,3.300]	0.223[0.208,0.231]
\mathcal{H}_2	$g = 0.2$	20-28	3	3	0.31	23.229[23.131,23.422]	0.855[0.691,0.921]	2.513[1.593,3.418]	0.222[0.197,0.232]

Since $\epsilon_{\mathbf{r}}$ is statistically equivalent for different lattice points \mathbf{r} , an ensemble of h_2 defined in Eq. (94) is statistically invariant under the combination of transposition and the π -rotation. The symmetry in Eqs. (60) and (95) requires the LEs of h_2 along the x direction to come in opposite-sign pairs, giving rise to $\nu_x = 0$. The hopping along the y direction and the hopping along the z direction are symmetric in Eq. (94). Thus, after transposition, we can also apply a mirror operation with respect to the plane with fixed $y + z$:

$$\mathcal{U}_{(r_x, r_y, r_z | r'_x, r'_y, r'_z)} = \delta_{r_x, r'_x} \delta_{r_y, -r'_z} \delta_{r_z, -r'_y}. \quad (96)$$

Transposition exchanges $t'_{\parallel} + t_{\parallel}$ and $t'_{\parallel} - t_{\parallel}$ and the mirror operation puts them back. Thus, an ensemble of h_2 is statistically invariant under the combination of transposition and the mirror operation. The symmetry in Eqs. (60) and (96) requires the LEs of h_2 along the $r_{(0,1,-1)} \equiv r_y - r_z$ direction to come in opposite-sign pairs, leading to $\nu_y = \nu_z$.

For the directions with non-zero weak topological indices [i.e., z direction in Eq. (39) and y, z directions in Eq. (94)], we calculate the LEs of the right-upper part [i.e., h in Eq. (39) and h_2 in Eq. (94)] as a function of the disorder strength W . In all these models, the distributions of the LEs for large L show the W -dependence described in Fig. 7. For $W = 0$, the $2L^2$ LEs form a continuum spectrum in the large L limit, including zero $\gamma = 0$. When W increases, the spectrum splits into the two continuous spectra. For $W > W_c^{(z)}$, all the L^2 LEs in the lower spectrum become negative. The non-localized region extends from $W = 0$ to $W = W_c^{(z)}$, while the Anderson insulator phase appears in $W > W_c^{(z)}$. $W_c^{(z)}$ is determined by the finite-size scaling of $\gamma_{\max}^{(1)}$ as in Sec. I G, which is summarized in Table VII.

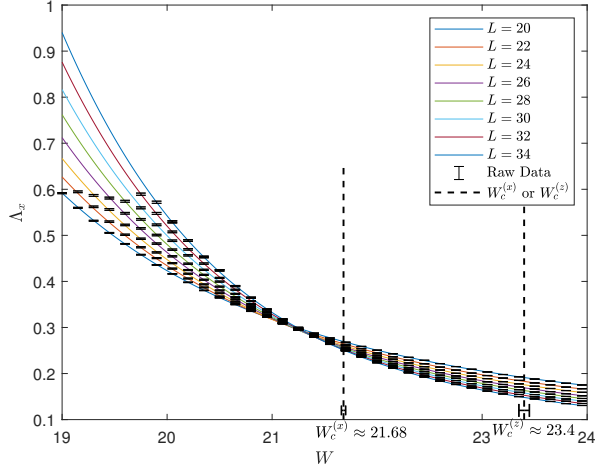
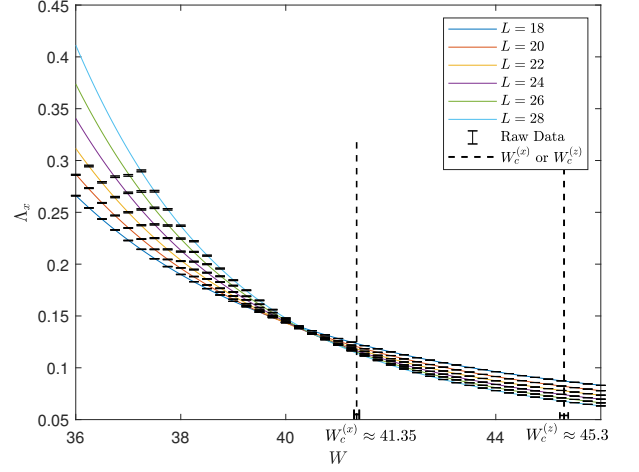
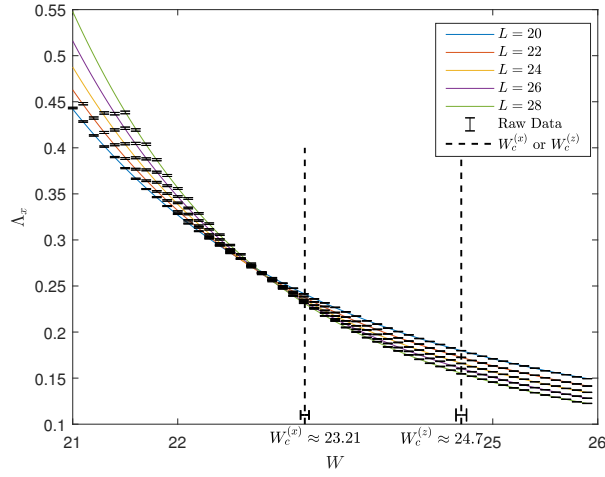
(a) nodal-line semimetal with $\nu_z \neq 0$ and $\nu_x = \nu_y = 0$ ($g = 0.22$)(b) nodal-line semimetal with $\nu_z \neq 0$ and $\nu_x = \nu_y = 0$ ($g = 1$)(c) nodal-line semimetal with $\nu_y = \nu_z \neq 0$ and $\nu_x = 0$

FIG. 8. Normalized localization length $\Lambda_x \equiv \xi_x/L$ along the x direction as a function of the disorder strength W for different system sizes L . (a, b) Nodal-line semimetal model in Eq. (33) with $\Delta = 0$, $t_{\parallel} = \sinh g$, $t'_{\parallel} = \cosh g$ [(a) $g = 0.22$ and (b) $g = 1$], $t_{\perp} = 1$, and (c) nodal-line semimetal model in Eq. (93) with $\Delta = 0$, $t_{\parallel} = \cosh g$, $t'_{\parallel} = \sinh g$ ($g = 0.2$), $t_{\perp} = 1$. The black points are the raw data with the error bars. The solid lines for different L and the dashed vertical line $W_c^{(x)}$ with the error bars are the results of the fitting according to Eqs. (20) and (21) with $(m, n) = (2, 3)$. The dashed line $W_c^{(z)}$ is evaluated by the fitting of the Lyapunov exponents along the z direction by Eqs. (74) and (75).

For the directions with zero weak topological indices [i.e., x, y directions in Eq. (39) and x direction in Eq. (94)], we calculate the localization length ξ_x in the quasi-1D geometry ($L_x \times L \times L$, $L_x \gg L$). Figure 8 shows the normalized localization length $\Lambda_x \equiv \xi_x/L$ as a function of the disorder strength W . In all these models, Λ_x shows scale-invariant behavior inside the non-localized region. Fitting Λ_x around the scale-invariant points by the scaling functions of Eqs. (20) and (21), we evaluate the critical exponent ν and the critical disorder strength $W_c^{(x)}$, as summarized in Table VI. The critical disorder strength $W_c^{(x)}$ is far below $W_c^{(z)}$, demonstrating the presence of the quasi-localized phases for $W_c^{(x)} < W < W_c^{(z)}$ in these three models (Table VII). The evaluated critical exponents are consistent with the critical exponent $\nu = 0.820[0.783, 0.846]$ shown in the main text for the nodal-line semimetal in class BDI. This consistency suggests that all the phase transitions between the metal and quasi-localized phases in the 3D models in symmetry class BDI are of the same nature.

Note also that ν in the nodal-line semimetal model of Eq. (39) with $t_{\parallel} = \cosh g$, $t'_{\parallel} = \sinh g$ ($g = 0.22$) shows the

TABLE VII. Comparison of the two critical disorder strengths, $W_c^{(x)}$ and $W_c^{(z)}$, in the nodal-line semimetal models \mathcal{H} [Eq. (33)] and \mathcal{H}_2 [Eq. (93)]. The parameters of these models are the same as in Table VI. Both models are characterized by the parameters $\Delta = 0$, $t_{\parallel} = \sinh g$, $t'_{\parallel} = \cosh g$, $t_{\perp} = 1$. The column “parameter” specifies the value of g . In the two models, the non-localized regions extend from $W = 0$ to $W = W_c^{(z)}$, and the quasi-localized phases extend from $W_c^{(x)}$ to $W_c^{(z)}$.

symmetry class	model	parameter	$W_c^{(x)}$	$W_c^{(z)}$
BDI	\mathcal{H}	$g = 0.22$	21.73[21.66,21.80]	23.4[23.3,23.5]
BDI	\mathcal{H}_2	$g = 1$	41.36[41.26,41.46]	45.3[45.2,45.4]
BDI	\mathcal{H}_2	$g = 0.2$	23.23[23.13,23.42]	24.7[24.6,24.8]

larger error bars in their fitting results (see Table VI). These larger error bars may stem from a severe crossover effect. For $t'_{\parallel} = \sinh g = 0$, the nodal-line semimetal model has an extra unitary symmetry $\mathcal{H} = \sigma_z \mathcal{H} \sigma_z$. The Hamiltonian can be block-diagonalized into two parts, and each block belongs to orthogonal class. For nonzero but small g , this unitary symmetry is only weakly broken. Thus, the finite-size systems with smaller g must suffer from a stronger crossover effect.

3. Weak topological insulators and ordinary insulators in class BDI

Zero-energy states of the nodal-line semimetal model in Eq. (33) can be either in a topological insulator state with $(\nu_x, \nu_y, \nu_z) = (0, 0, 1)$ or in an ordinary insulator state with $(\nu_x, \nu_y, \nu_z) = (0, 0, 0)$, depending on its tight-binding parameters. For simplicity, we assume $\Delta, t_{\perp}, t_{\parallel} > 0$ in Eq. (33). For $\Delta + 4t_{\perp} < 2|t'_{\parallel}|$ ($\Delta - 4t_{\perp} > 2|t'_{\parallel}|$), the zero-energy states of \mathcal{H} in Eq. (33) are in the topological (ordinary) insulator state in the clean limit ($W = 0$).

In Ref. [50], the localization lengths of Eq. (33) along the x direction were calculated with the quasi-1D geometry ($L_x \times L \times L$, $L_x \gg L$), and the two consecutive disorder-driven phase transitions were identified for the following set of parameters:

$$t_{\perp} = 3/10, \quad t'_{\parallel} = 1, \quad t_{\parallel} = 1/4, \quad \Delta = 1/2 \quad (\text{topological insulator in the clean limit}). \quad (97)$$

The two phase transitions are i) a transition from the topological insulator phase to the diffusive metal phase at $W_{c,1}^{(x)} = 3.135$ [3.132, 3.138] and ii) a transition from the diffusive metal phase to the Anderson insulator phase at $W_{c,2}^{(x)} = 11.96$ [11.92, 12.02], respectively. In addition, Ref. [50] studied another parameter set,

$$t_{\perp} = 3/10, \quad t'_{\parallel} = 1, \quad t_{\parallel} = 1/4, \quad \Delta = 4 \quad (\text{ordinary insulator in the clean limit}), \quad (98)$$

where a disorder-driven phase transition from the 3D ordinary band insulator phase to the diffusive metal phase [Fig. 9(b)] was found at $W_{c,3}^{(x)} = 4.76$ [4.75, 4.77]. The normalized localization length $\Lambda_x \equiv \xi_x/L$ shows scale-invariant behavior at these critical disorder strengths. From the finite-size scaling analyses, it was clarified that these phase transitions are universally characterized by the same critical exponent $\nu = 0.82 \pm 0.04$ [50], which is consistent with the evaluations of the disordered nodal-line semimetal models studied in the main text.

For these two sets of parameters, we study the localization length and the winding number along the z direction. We calculate the LEs of the right-upper part h of \mathcal{H} in the canonical basis [i.e., Eq. (39)] with the quasi-1D geometry ($L \times L \times L_z$, $L_z \gg L$). For the parameters in Eq. (97), the LEs show a W -dependence described as Fig. 9(c). The topological insulator is stable under weak disorder. For $W < W_{c,1}^{(z)}$, all the $2L^2$ LEs are positive, and the localization length is finite. The winding number w_z along the z direction is L^2 , giving rise to $\nu_z = 1$. The non-localized region appears from $W = W_{c,1}^{(z)}$ to $W = W_{c,2}^{(z)}$ ($> W_{c,1}^{(z)}$), where a continuous spectrum of LEs includes zero $\gamma = 0$. When W increases from $W_{c,1}^{(z)}$ to $W_{c,2}^{(z)}$, L^2 positive LEs cross zero and become negative; ν_z changes from 1 to 0. For $W > W_{c,2}^{(z)}$, the L^2 LEs are positive and the other L^2 LEs are negative, leading to $\nu_z = 0$. For the parameters in Eq. (98), the LEs shows a W -dependence described as Fig. 9(d), where the non-localized region appears from $W = W_{c,3}^{(z)}$ to $W = W_{c,4}^{(z)}$ ($> W_{c,3}^{(z)}$). In the non-localized region, the number of positive LEs is greater than the number of negative ones, leading to $\nu_z > 0$.

From the finite-size scaling analyses of the minimal or maximal LEs by Eqs. (74), (75), or (89), we determine the phase boundaries of the non-localized regions as $W_{c,1}^{(z)} = 3.08$ [3.07, 3.09], $W_{c,2}^{(z)} = 13.3$ [13.2, 13.4], and $W_{c,3}^{(z)} = 4.56$ [4.55, 4.57] (see Table VIII). From a comparison of these numbers with $W_c^{(x)}$ obtained in Ref. [50] (see Table IX), we conclude that the quasi-localized phases appear inside the non-localized regions:

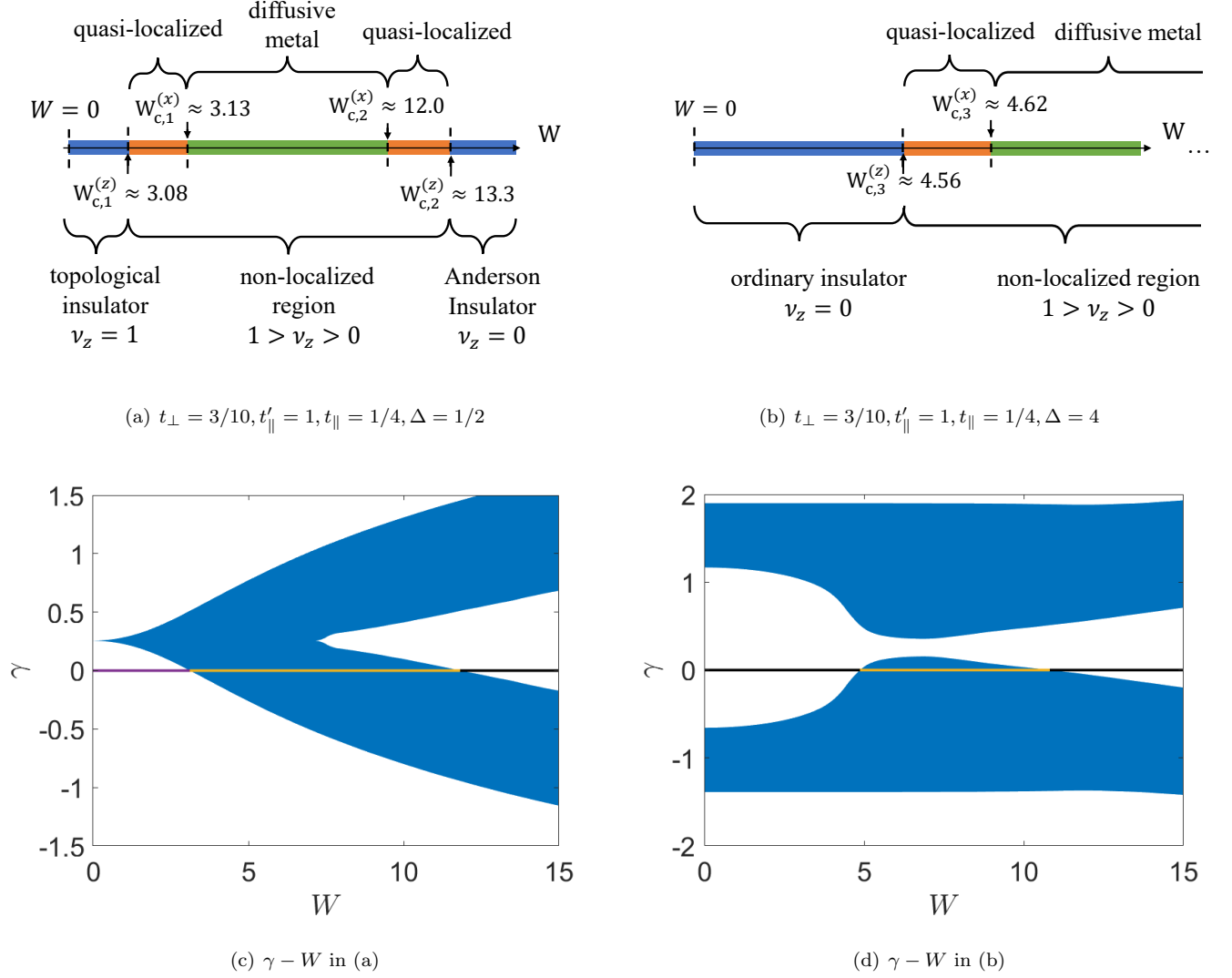


FIG. 9. (a,b) Schematic phase diagrams of \mathcal{H} in different parameter sets, (a) weak topological and (b) ordinary insulator sides. $W_{c,i}^{(x)}$ ($i = 1, 2, 3$) stand for critical points of the Anderson transitions in the x or y direction [50]. The weak topological index ν_z is finite for $W_{c,1}^{(z)} < W < W_{c,2}^{(z)}$ of (a) and for $W_{c,3}^{(z)} < W$ of (b). The $2L^2$ Lyapunov exponents of h in the same parameter sets as (a) and (b) are shown in (c) and (d), respectively.

$$\begin{cases} W < W_{c,1}^{(z)} & \text{(topological insulator phase),} \\ W_{c,1}^{(z)} < W < W_{c,1}^{(x)} & \text{(quasi-localized phase),} \\ W_{c,1}^{(x)} < W < W_{c,2}^{(x)} & \text{(diffusive metal phase),} \\ W_{c,2}^{(x)} < W < W_{c,2}^{(z)} & \text{(quasi-localized phase),} \\ W_{c,2}^{(z)} < W & \text{(Anderson insulator phase),} \end{cases} \quad (99)$$

for the parameters in Eq. (97) and

$$\begin{cases} W < W_{c,3}^{(z)} & \text{(ordinary insulator phase),} \\ W_{c,3}^{(z)} < W < W_{c,3}^{(x)} & \text{(quasi-localized phase),} \\ W_{c,3}^{(x)} < W < \dots & \text{(diffusive metal phase),} \end{cases} \quad (100)$$

for Eq. (98). Here, “...” means that when W is further increased, the system undergoes a transition from the diffusive metal phase to the quasi-localized phase at $W_{c,4}^{(x)}$, and a transition from the quasi-localized phase to the Anderson

TABLE VIII. Finite-size scaling analyses of $\gamma_{\max}^{(1)}(W, L)$ or $\gamma_{\min}^{(1)}(W, L)$ for the several disorder strength W around $W = W_c^{(z)}$ for the disordered topological insulator model with the parameters in Eq. (97) (shown as “P1” in the “parameter set”), and the disordered ordinary insulator model with the parameters in Eq. (98) (shown as “P3” in the “parameter set”). The square brackets are the 95% confidence error bars determined by the Monte Carlo analyses.

parameter set	W	L	$\gamma_{\min}^{(1)}(W, L)$		a	GOF
P1	3.07	24 - 60	0.0013	[0.0012, 0.0014]	0.050 [0.046, 0.053]	0.64
P1	3.08	24 - 60	-0.0002	[-0.0003, -0.0000]	0.051 [0.047, 0.054]	0.90
P1	3.09	24 - 60	-0.0015	[-0.0016, -0.0014]	0.048 [0.045, 0.051]	0.46

parameter set	W	L	$\gamma_{\max}^{(1)}(W, L)$		a	GOF
P1	13.2	14 - 28	0.006	[0.002, 0.010]	-0.967 [-1.048, -0.889]	0.15
P1	13.3	14 - 28	0.0007	[-0.003, 0.004]	-0.954 [-1.027, -0.880]	0.74
P1	13.4	14 - 28	-0.006	[-0.010, -0.002]	-0.951 [-1.026, -0.870]	0.11
P3	4.60	14 - 28	-0.007	[-0.011, -0.0028]	-1.177 [-1.257, -1.097]	0.74
P3	4.62	14 - 28	-0.003	[-0.007, 0.001]	-1.091 [-1.163, -1.009]	0.19
P3	4.63	14 - 28	0.007	[0.002, 0.0109]	-1.150 [-1.231, -1.064]	0.79

TABLE IX. Comparison of the critical disorder strengths, $W_c^{(z)}$ and $W_c^{(x)}$, in the disordered topological insulator model with the parameters in Eq. (97) (shown as “T1” and “T2” in the “transition”), and the disordered ordinary insulator model with the parameters in Eq. (98) (shown as “T3” in the “transition”). The square brackets are the 95% confidence error bars determined by the synthetic data.

symmetry class	transition	$W_c^{(x)}$	$W_c^{(z)}$
BDI	T1	3.135[3.132, 3.138] ^a	3.08[3.07, 3.09]
BDI	T2	11.96[11.92, 12.02] ^a	13.3[13.2, 13.4]
BDI	T3	4.62[4.60, 4.63] ^a	4.56[4.55, 4.57]

^a from Ref. [50]

insulator phase at $W_{c,4}^{(z)}$, but the respective critical disorder strengths $W_{c,4}^{(x)}$ and $W_{c,4}^{(z)}$ are not determined. The phase diagrams of the disordered topological insulator and ordinary insulator are shown in Figs. 9(a) and 9(b).

I. Anderson transitions in chiral-symmetric models with no weak topological indices

For comparison, we study three-dimensional (3D) chiral-symmetric models in symmetry classes BDI and AIII, where statistical symmetries enforce all the three topological indices to be zero. We refer to these models as non-topological models. Notably, the disordered ordinary insulator model in Eq. (33) with the parameters in Eq. (98) is a topological model because non-zero ν_z is induced by the disorder [see also Figs. 9(d) and 9(b)]. Non-topological models have the following three features that are distinct from the topological models in the same chiral symmetry classes:

1. In the quasi-1D geometry ($L \times L \times L_\mu$, $L_\mu \gg L$), the localization length along any spatial direction is always finite with finite L . In the topological models with $\nu_z \neq 0$, the localization length along the z direction can diverge for finite L when the 1D winding w_z changes.
2. In the thermodynamic limit $L \rightarrow \infty$, the localization lengths along all the spatial directions diverge at the same critical point, which implies no quasi-localized phase. In the topological models, the localization length along the z direction and those along the other two directions diverge at different critical points in the thermodynamic limit, which gives rise to the quasi-localized phase.
3. The divergence of the localization length along all the directions is characterized by the same critical exponent in the non-topological models. In the topological models, the divergence of the localization length along the z direction and those along the other directions are characterized by the different critical exponents. The two exponents in the topological models are also different from the exponents in the non-topological models in the same symmetry class.

1. Three-dimensional non-topological models in classes BDI and AIII

Let us introduce the following non-topological chiral-symmetric model that belongs to symmetry class BDI or AIII,

$$\mathcal{H}_0 = \sum_{\mathbf{r}=(x,y,z)} \left\{ (\Delta + \epsilon_{\mathbf{r}}) c_{\mathbf{r}}^\dagger \sigma_z c_{\mathbf{r}} + \epsilon'_{\mathbf{r}} c_{\mathbf{r}}^\dagger \sigma_y c_{\mathbf{r}} + \left[\sum_{\mu=x,y} \left(t_\perp c_{\mathbf{r}+\mathbf{e}_\mu}^\dagger \sigma_0 c_{\mathbf{r}} \right) + t_\parallel c_{\mathbf{r}+\mathbf{e}_z}^\dagger \sigma_z c_{\mathbf{r}} + it'_\parallel c_{\mathbf{r}+\mathbf{e}_z}^\dagger \sigma_y c_{\mathbf{r}} + \text{H.c.} \right] \right\}, \quad (101)$$

where $c_{\mathbf{r}}$ is a two-component annihilation operator at the cubic-lattice site $\mathbf{r} \equiv (r_x, r_y, r_z)$, \mathbf{e}_μ 's ($\mu = x, y, z$) are the unit vectors connecting the nearest neighbor cubic-lattice sites, σ_μ 's ($\mu = 0, x, y, z$) are the two-by-two unit matrix and Pauli matrices for the two orbitals, $\Delta, t_\perp, t_\parallel, t'_\parallel$ are the real parameters, and $\epsilon_{\mathbf{r}}$ and $\epsilon'_{\mathbf{r}}$ are the real-valued on-site random potential. We choose the parameters to be $\Delta = 0, t_\perp = 1, t_\parallel = 13/12, t'_\parallel = 5/12$. The model in the clean limit ($\epsilon_{\mathbf{r}} \equiv \epsilon'_{\mathbf{r}} \equiv 0$) has a finite density of states at $E = 0$. \mathcal{H}_0 respects chiral symmetry, $\mathcal{H}_0 = -\mathcal{C}^\dagger \mathcal{H}_0 \mathcal{C}$ with the chiral operator

$$\mathcal{C}_{\mathbf{r},\mathbf{r}'} \equiv (-1)^{x+y} \delta_{\mathbf{r},\mathbf{r}'} \sigma_x, \quad (102)$$

satisfying $\mathcal{C} = \mathcal{C}^T$. For $\epsilon'_{\mathbf{r}} = 0$, \mathcal{H}_0 respects time-reversal symmetry $\mathcal{H}_0 = \mathcal{H}_0^*$ and hence belongs to the chiral orthogonal class (class BDI). For $\epsilon'_{\mathbf{r}} \neq 0$, time-reversal symmetry is broken, and \mathcal{H}_0 belongs to the chiral unitary class (class AIII). For \mathcal{H}_0 in class BDI, we choose $\epsilon_{\mathbf{r}}$ to be uniformly distributed in $[-W/2, W/2]$. For \mathcal{H}_0 in class AIII, on the other hand, we choose $\epsilon_{\mathbf{r}}$ and $\epsilon'_{\mathbf{r}}$ to be uniformly distributed for $\epsilon_{\mathbf{r}}^2 + \epsilon'_{\mathbf{r}}{}^2 \leq W^2$.

Following Eq. (28), we decompose \mathcal{H}_0 into the block-off-diagonal structure in a basis that diagonalizes the chiral operator \mathcal{C} . The right-upper part h_0 of \mathcal{H}_0 is regarded as a single-orbital tight-binding model on the cubic lattice,

$$h_0 = \sum_{\mathbf{r}} \left[(\Delta + \epsilon_{\mathbf{r}} + i\epsilon'_{\mathbf{r}}) f_{\mathbf{r}}^\dagger f_{\mathbf{r}} + \sum_{\mu=x,y} \left(t_\perp f_{\mathbf{r}+\mathbf{e}_\mu}^\dagger f_{\mathbf{r}} + \text{H.c.} \right) + \left(t_\parallel - (-1)^{r_x+r_y} t'_\parallel \right) f_{\mathbf{r}+\mathbf{e}_z}^\dagger f_{\mathbf{r}} + \left(t_\parallel + (-1)^{r_x+r_y} t'_\parallel \right) f_{\mathbf{r}}^\dagger f_{\mathbf{r}+\mathbf{e}_z} \right]. \quad (103)$$

Transposition exchanges $t_\parallel - (-1)^{r_x+r_y} t'_\parallel$ and $t_\parallel + (-1)^{r_x+r_y} t'_\parallel$ in h_0 . Thus, as a unitary transformation in Eqs. (60) and (61), we apply a spatial translation along the x or y direction by \mathbf{e}_x or \mathbf{e}_y ,

$$\mathcal{U}_{(r_x, r_y, r_z | r'_x, r'_y, r'_z)} = \begin{cases} \delta_{r_x, r'_x+1} \delta_{r_y, r'_y} \delta_{r_z, r'_z}, \\ \delta_{r_x, r'_x} \delta_{r_y, r'_y+1} \delta_{r_z, r'_z}. \end{cases} \quad (104)$$

Instead of Eq. (104), we can also use a mirror operation with respect to the $r_x = 1/2$ plane or the $r_y = 1/2$ plane

$$\mathcal{U}_{(r_x, r_y, r_z | r'_x, r'_y, r'_z)} = \begin{cases} \delta_{r_x+r'_x, 1} \delta_{r_y, r'_y} \delta_{r_z, r'_z}, \\ \delta_{r_x, r'_x} \delta_{r_y+r'_y, 1} \delta_{r_z, r'_z}. \end{cases} \quad (105)$$

Since $\epsilon_{\mathbf{r}}$ ($\epsilon'_{\mathbf{r}}$) at different lattice points \mathbf{r} is statistically equivalent, an ensemble of h_0 defined in Eq. (103) is statistically invariant under the combination of transposition and any of these unitary transformations. These statistical symmetries require the LEs of h_0 along all the directions to come in opposite-sign pairs, leading to $\nu_x = \nu_y = \nu_z = 0$.

For \mathcal{H}_0 in symmetry class BDI, we calculate the localization lengths ξ_x, ξ_z along the x, z directions with the quasi-1D geometry $L^2 \times L_\mu$ ($\mu = x, z; L_\mu \gg L$). Because of chiral symmetry, it is sufficient to calculate the product of the transfer matrices of h_0 [see Eq. (31)]. Because of the statistical symmetries, the LEs of h_0 come in opposite-sign pairs. Both normalized localization length $\Lambda_x \equiv \xi_x/L$ and $\Lambda_z \equiv \xi_z/L$ show scale-invariant behavior around the same critical disorder strength $W \approx 23$ (see Fig. 10). From the fitting by the polynomial expansion of the finite-size scaling function [Eqs. (20) and (21)], we determine the critical disorder strength and the critical exponent (see the fourth to seventh rows of Table III). The critical disorder strength and exponent determined from Λ_z and those determined from Λ_x are consistent with each other. The critical exponent is $\nu = 1.089 [1.005, 1.128]$, and different from the two exponents ($\nu = 0.820 [0.787, 0.848]$ and $\nu' = 1$) of the topological model in the same symmetry class (i.e., class BDI). Reference [71] studied the localization length of \mathcal{H}_0 along the z direction with the different parameters $\Delta = t_\perp = t'_\parallel = 1, t_\parallel = 1/2$ and evaluated the critical exponent to be $\nu = 1.119 [0.973, 1.241]$, which is consistent with our evaluation.

For \mathcal{H}_0 in symmetry class AIII, we calculate the normalized localization length $\Lambda_z = \xi_z/L$ with the quasi-1D geometry $L^2 \times L_z$ and $L_z \gg L$. Λ_z shows scale-invariant behavior around the critical disorder strength $W \approx 8$ (see Fig. 11). From the fitting by the polynomial expansion of the finite-size scaling function [Eqs. (20 and (21)], we determine the critical disorder strength and critical exponents. The critical exponent is $\nu = 1.024 [0.973, 1.070]$ (see the last row of Table III) and different from the two critical exponents $\nu = 0.824 [0.776, 0.862]$ and $\nu' = 1$ of the topological model in the same symmetry class (i.e., class AIII).

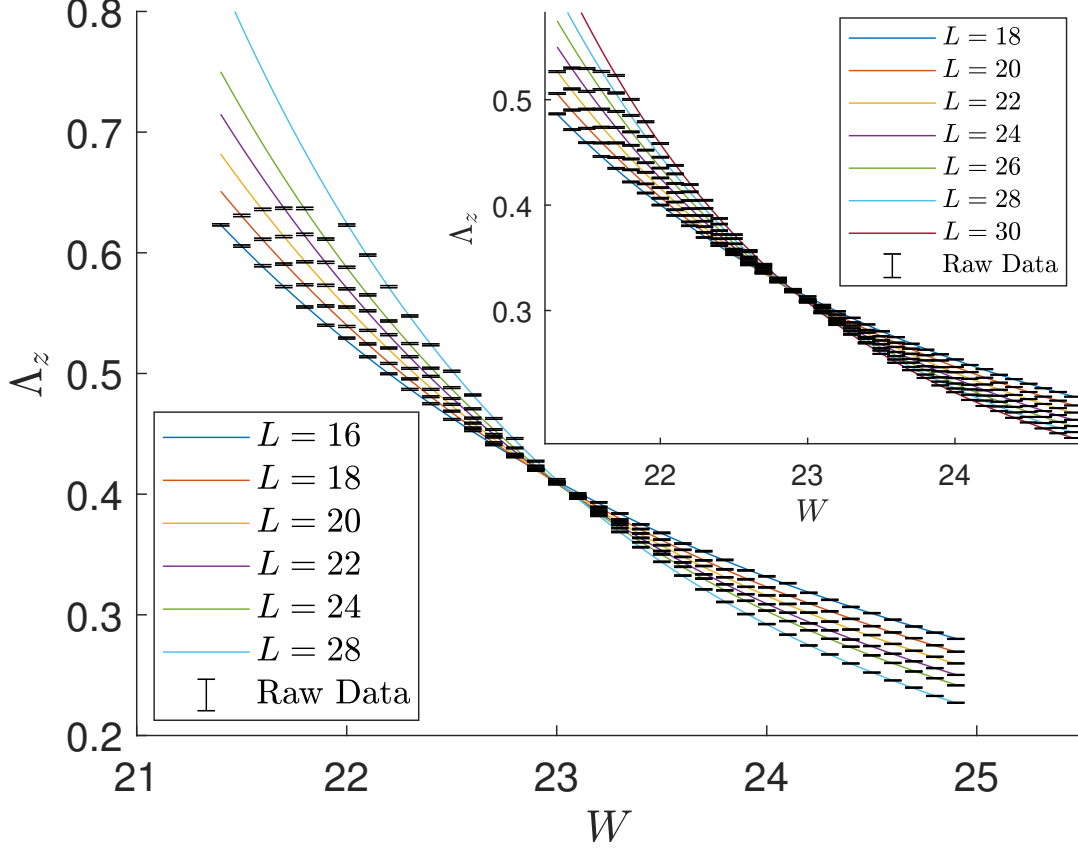


FIG. 10. Normalized localization length $\Lambda_z \equiv \xi_z/L$ along the z direction as a function of the disorder strength W in the non-topological model \mathcal{H}_0 ($\Delta = 0, t_\perp = 1, t_\parallel = 13/12, t'_\parallel = 5/12$) in class BDI [Eq. (101)] with the quasi-1D geometry ($L \times L \times L_z$). The black points are the raw data with the error bars. The solid lines for different L are the results of the fitting according to Eqs. (20) and (21) with $(m, n) = (2, 3)$. Inset: $\Lambda_x \equiv \xi_x/L$ as a function of W in the same model.

2. Another three-dimensional non-topological model in class AIII

Reference [71] introduced another 3D non-topological model in symmetry class AIII,

$$\mathcal{H}'_0 = \sum_{\mathbf{r}=(r_x, r_y, r_z)} \left\{ (\Delta + \epsilon_{\mathbf{r}}) c_{\mathbf{r}}^\dagger \sigma_z c_{\mathbf{r}} + \left[c_{\mathbf{r}+\mathbf{e}_x}^\dagger (t_1 \sigma_z + i t_\perp \sigma_x) c_{\mathbf{r}} + c_{\mathbf{r}+\mathbf{e}_y}^\dagger (t_2 \sigma_0 + i t_\perp \sigma_y) c_{\mathbf{r}} + t_\parallel c_{\mathbf{r}+\mathbf{e}_z}^\dagger \sigma_0 c_{\mathbf{r}} + \text{H.c.} \right] \right\}, \quad (106)$$

where the disorder potential $\epsilon_{\mathbf{r}}$ distributes uniformly in $[-W/2, W/2]$, and the parameters are chosen to be $\Delta = 0, t_\perp = 3/5, t_\parallel = 2/5, t_1 = t_2 = 1/2$. \mathcal{H}'_0 respects chiral symmetry $\mathcal{H}'_0 = -C^\dagger \mathcal{H}'_0 C$ with a chiral operator C

$$C_{\mathbf{r}, \mathbf{r}'} \equiv (-1)^{y+z} \delta_{\mathbf{r}, \mathbf{r}'} \sigma_y. \quad (107)$$

In terms of Eq. (28), \mathcal{H}'_0 is decomposed into the block off-diagonal structure in a basis that diagonalizes the chiral operator. The right-upper part h'_0 of \mathcal{H}'_0 in this basis is given by a single-orbital tight-binding model on the cubic lattice site,

$$h'_0 = \sum_{\mathbf{r}=(r_x, r_y, r_z)} \left[(\Delta + \epsilon_{\mathbf{r}}) f_{\mathbf{r}}^\dagger f_{\mathbf{r}} + (t_1 + (-1)^{r_y+r_z} t_\perp) f_{\mathbf{r}+\mathbf{e}_x}^\dagger f_{\mathbf{r}} + (t_1 - (-1)^{r_y+r_z} t_\perp) f_{\mathbf{r}}^\dagger f_{\mathbf{r}+\mathbf{e}_x} \right. \\ \left. + (t_2 - (-1)^{r_y+r_z} i t_\perp) f_{\mathbf{r}+\mathbf{e}_y}^\dagger f_{\mathbf{r}} + (t_2 - (-1)^{r_y+r_z} i t_\perp) f_{\mathbf{r}}^\dagger f_{\mathbf{r}+\mathbf{e}_y} + \left(t_\parallel f_{\mathbf{r}+\mathbf{e}_z}^\dagger f_{\mathbf{r}} + \text{H.c.} \right) \right]. \quad (108)$$

Hermitian conjugation exchanges $t_1 + (-1)^{r_y+r_z} t_\perp$ and $t_1 - (-1)^{r_y+r_z} t_\perp$, but transforms $t_2 - (-1)^{r_y+r_z} i t_\perp$ into $t_2 + (-1)^{r_y+r_z} i t_\perp$. Thus, as a unitary transformation in Eqs. (61) and (68), we apply a spatial translation along the y or

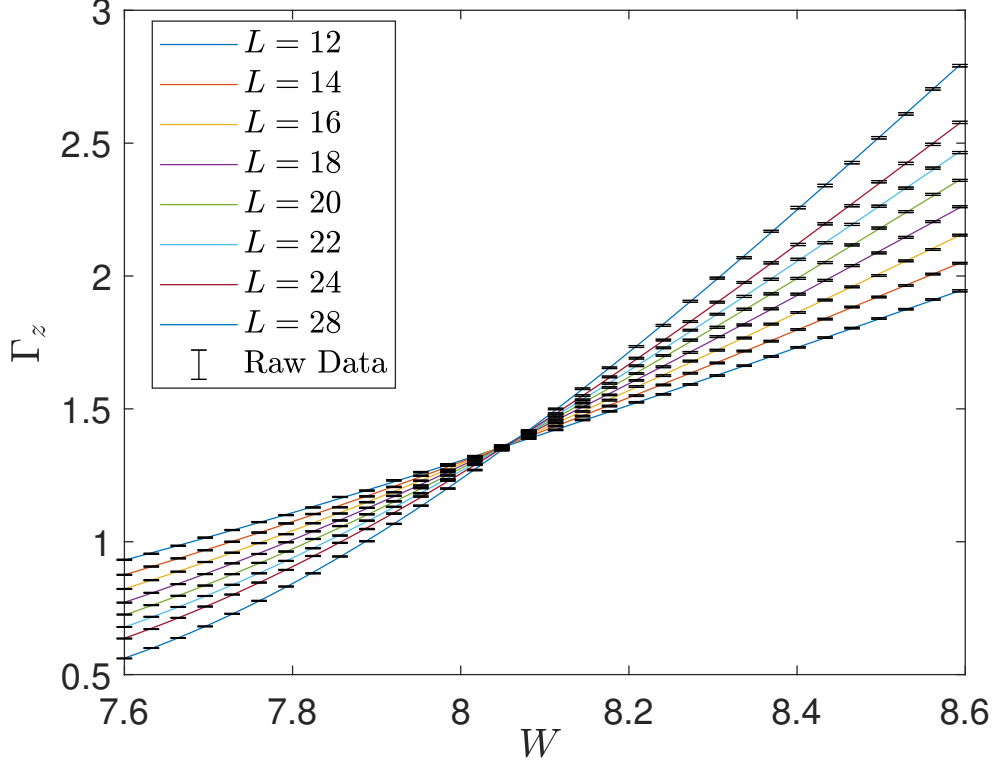


FIG. 11. Inverse $\Gamma_z \equiv 1/\Lambda_z \equiv \xi_z/L$ of the normalized localization length along the z direction as a function of the disorder strength W in the non-topological model \mathcal{H}' ($\Delta = 0, t_\perp = 1, t_\parallel = 13/12, t'_\parallel = 5/12$) in class AIII [Eq. (101)] with the quasi-1D geometry ($L \times L \times L_z$). The black points are the raw data with the error bars. The solid lines for different L are the results of the fitting according to Eqs. (20 and (21) with $(m, n) = (2, 3)$.

z direction by \mathbf{e}_y or \mathbf{e}_z ,

$$\mathcal{U}_{(r_x, r_y, r_z | r'_x, r'_y, r'_z)} = \begin{cases} \delta_{r_x, r'_x} \delta_{r_y, r'_y+1} \delta_{r_z, r'_z}, \\ \delta_{r_x, r'_x} \delta_{r_y, r'_y} \delta_{r_z, r'_z+1}. \end{cases} \quad (109)$$

Instead of Eq. (109), we can also use a mirror operation with respect to the $r_y = 1/2$ plane and the $r_z = 1/2$ plane,

$$\mathcal{U}_{(r_x, r_y, r_z | r'_x, r'_y, r'_z)} = \begin{cases} \delta_{r_x, r'_x} \delta_{r_y+r'_y, 1} \delta_{r_z, r'_z}, \\ \delta_{r_x, r'_x} \delta_{r_y, r'_y} \delta_{r_z+r'_z, 1}. \end{cases} \quad (110)$$

Since $\epsilon_{\mathbf{r}}$ is statistically equivalent for different lattice points \mathbf{r} , an ensemble of h'_0 defined in Eq. (108) is statistically invariant under the combination of Hermitian conjugation and any of these unitary transformations. These symmetries require the LEs of h'_0 along all the directions to come in opposite-sign pairs, leading to $\nu_x = \nu_y = \nu_z = 0$. Reference [71] evaluated the critical exponent to be 1.059 [1.022, 1.100], which is consistent with our evaluation of the exponent in the non-topological model in symmetry class AIII.

J. Conductance and weak topological indices

In this section, we provide detailed numerical results of the two-terminal dimensionless conductance g in the quasi-localized, metallic, and Anderson-localized phases. We show that the quasi-localized phase is characterized by the finite conductance along the direction with the divergent localization length and the vanishing conductance along the other directions. By contrast, the metallic and Anderson-localized phases exhibit the finite and vanishing conductance along all the directions, respectively. We also demonstrate large sample fluctuations of the conductance along the direction with the divergent length. These unique properties in the quasi-localized phase are of direct relevance to

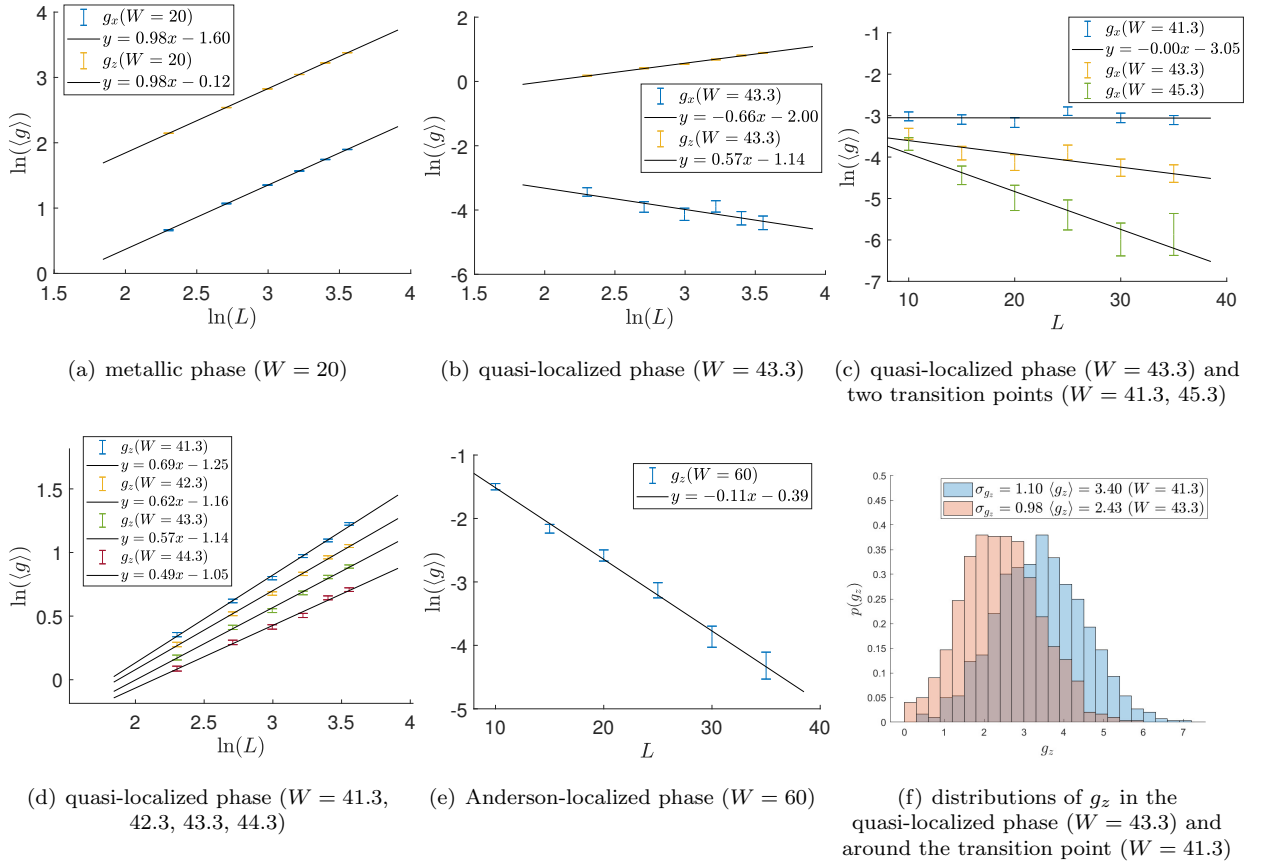


FIG. 12. (a)-(e) System-size dependence of the mean conductance $\langle g_\mu \rangle$ ($\mu = x, z$) of the nodal-line Hamiltonian [Eq. (33)] with $\nu_x = \nu_y = 0$ and $\nu_z \neq 0$. The mean conductance for the different cubic system sizes L^3 is plotted as a function of L (maximal size $L = 35$) (a) in the metallic phase ($W = 20$), (b) in the quasi-localized phase ($W = 43.3$), (c) in the quasi-localized phase ($W = 43.3$) and around the two transition points ($W = 41.3 \approx W_c^{(x)}$, $W = 45.3 \approx W_c^{(z)}$), (d) in the quasi-localized phase ($41.3 < W < 45.3$), (e) in the Anderson-localized phase ($W = 60$). We calculate the conductance of $N = 1000$ samples for each cubic system size and disorder strength W . The error bars of $\langle g_\mu \rangle$ are estimated as $\sqrt{(\langle g_\mu^2 \rangle - \langle g_\mu \rangle^2)/N}$. (f) Distributions of g_z in the quasi-localized phase ($W = 43.3$) and around the transition point ($W = 41.3 \approx W_c^{(x)}$). The distributions are evaluated for the maximal system size $L = 35$. $\sigma_{g_z} = \sqrt{\langle g_z^2 \rangle - \langle g_z \rangle^2}$ is the standard deviation of g_z .

transport experiments. In fact, g is directly related to the electric conductance G and thermal conductance G_T by $hG = e^2 g$ and $hG_T \propto k_B^2 T g$, respectively, where h is the Planck constant, e is the elementary charge, k_B is the Boltzmann constant, and T is the temperature.

We calculate the two-terminal conductance g of the nodal-line Hamiltonian in Eq. (33) with $\nu_x = \nu_y = 0$ and $\nu_z \neq 0$ for the different disorder strength W . Here, g is obtained from the transmission matrix t by the transfer matrix method [84, 85], $g = \text{Tr}(t^\dagger t)$. To compute the transmission matrix t along the μ direction ($\mu = x, z$), we take the nodal-line Hamiltonian on a cubic lattice of size L^3 and couple it with two leads at its two ends. Each lead is composed of decoupled 1D metal wires along the μ direction,

$$\mathcal{H}_{\text{lead}} = -t_{\text{lead}} \sum_{\mathbf{r}=(r_x, r_y, r_z)} (c_{\mathbf{r}+\mathbf{e}_\mu}^\dagger \sigma_z c_{\mathbf{r}} + \text{H.c.}), \quad (111)$$

which respects the same time-reversal and chiral symmetries as the nodal-line Hamiltonian. We choose the parameters of the nodal-line Hamiltonian in Eq. (33) as $\Delta = 0$, $t_{\parallel} = \sinh 1$, $t'_{\parallel} = \cosh 1$, $t_{\perp} = 1$. The phase diagram of the Hamiltonian was obtained by the localization lengths along the x and z directions [see Fig. 8(b)]. As the disorder

strength W increases, the zero-energy states undergo the phase transitions:

$$\begin{cases} W < W_c^{(x)} \approx 41.3 & \text{(metallic phase);} \\ W_c^{(x)} < W < W_c^{(z)} \approx 45.3 & \text{(quasi-localized phase);} \\ W_c^{(z)} < W & \text{(localized phase).} \end{cases} \quad (112)$$

In the metallic phase ($W < 41.3$), both g_x and g_z show Ohm's law, $\langle g_\mu \rangle \propto L$ for $\mu = x, z$ [Fig. 12(a)]. Around the transition point between the metallic and quasi-localized phases ($W = 41.3$), $\langle g_x \rangle$ becomes scale-invariant [Fig. 12(c)], which is consistent with the scale-invariant behavior of the localization length along the x direction. In the quasi-localized phase ($41.3 < W < 45.3$), $\langle g_x \rangle$ decays exponentially with the system size L [see Fig. 12(c)]. In contrast, $\langle g_z \rangle$ grows with L in the power law, $\langle g_z \rangle \propto L^\alpha$, characterized by a non-universal exponent α ($0 < \alpha < 1$) [Figs. 12(b) and 12(d)]. Notably, g_z exhibits large sample fluctuations, and its standard deviation is comparable to the mean value [Fig. 12(f)]. In the Anderson-localized phase ($45.3 < W$), both g_x and g_z decay exponentially with L [Fig. 12(e)].
